RADIATION BOUNDARY CONDITIONS FOR MAXWELL'S EQUATIONS: A REVIEW OF ACCURATE TIME-DOMAIN FORMULATIONS

THOMAS HAGSTROM AND STEPHEN LAU

ABSTRACT. We review time-domain formulations of radiation boundary conditions for Maxwell's equations, focusing on methods which can deliver arbitrary accuracy at acceptable computational cost. Examples include fast evaluations of nonlocal conditions on symmetric and general boundaries, methods based on identfying and evaluating equivalent sources, and local approximations such as the perfectly matched layer and sequences of local boundary conditions. Complexity estimates are derived to assess work and storage requirements as a function of wavelength and simulation time.

1. INTRODUCTION

As the radiation of energy to the far field is an important feature of most problems in computational electromagnetics, an accurate and efficient truncation of the domain is a practical necessity for computations. In recent years there have been rapid developments in this field. In this review we will concentrate on strategies which can provide arbitrary accuracy. These include a variety of exact boundary condition formulations, which are all nonlocal in space and time, in addition to convergent local approximations such as the perfectly matched layer (PML). Besides describing the basic mathematical and algorithmic content of the various methods, we will, when possible, estimate their computational complexity as a function of the harmonic content of the field and the simulation time. Our goal is not to advocate one of the methods discussed over another. We will see that they are all capable of providing excellent accuracy at acceptable cost in many settings, and that an optimal choice will depend both on the details of the problem as well as on the time to be invested on code development.

We will assume that in the far field, that is beyond the computational domain Ω, we have a homogeneous, isotropic, dielectric material. In `cgs` units the source–free Maxwell equations then are:

$$\frac{\partial E}{\partial t} - c\nabla \times B = 0, \tag{1.1}$$

$$\frac{\partial B}{\partial t} + c\nabla \times E = 0, \tag{1.2}$$

1991 *Mathematics Subject Classification.* 65M99,78M99.

Supported in part by ARO Grant DAAD19-03-1-0146 and NSF Grant DMS-0610067. The second author was also supported by NSF Grant DMS-0554377. Any conclusions or recommendations expressed in this paper are those of the authors and do not necessarily reflect the views of ARO or NSF.

Report Documentation Page

Form Approved
OMB No. 0704-0188

1. REPORT DATE	2. REPORT TYPE	3. DATES COVERED
2007		**00-00-2007 to 00-00-2007**

4. TITLE AND SUBTITLE	5a. CONTRACT NUMBER
Radiation Boundary Conditions for Maxwell's Equations: A Review of Accurate Time-Domain Formulations	5b. GRANT NUMBER
	5c. PROGRAM ELEMENT NUMBER
6. AUTHOR(S)	5d. PROJECT NUMBER
	5e. TASK NUMBER
	5f. WORK UNIT NUMBER
7. PERFORMING ORGANIZATION NAME(S) AND ADDRESS(ES) **Brown University,Division of Applied Mathematics,182 George Street,Providence,RI,02912**	8. PERFORMING ORGANIZATION REPORT NUMBER
9. SPONSORING/MONITORING AGENCY NAME(S) AND ADDRESS(ES)	10. SPONSOR/MONITOR'S ACRONYM(S)
	11. SPONSOR/MONITOR'S REPORT NUMBER(S)

12. DISTRIBUTION/AVAILABILITY STATEMENT
Approved for public release; distribution unlimited

13. SUPPLEMENTARY NOTES

14. ABSTRACT

We review time-domain formulations of radiation boundary conditions for Maxwell's equations, focusing on methods which can deliver arbitrary accuracy at acceptable computational cost. Examples include fast evaluations of nonlocal conditions on symmetric and general boundaries, methods based on identfying and evaluating equivalent sources, and local approximations such as the perfectly matched layer and sequences of local boundary conditions. Complexity estimates are derived to assess work and storage requirements as a function of wavelength and simulation time.

15. SUBJECT TERMS

16. SECURITY CLASSIFICATION OF:			17. LIMITATION OF ABSTRACT	18. NUMBER OF PAGES	19a. NAME OF RESPONSIBLE PERSON
a. REPORT	b. ABSTRACT	c. THIS PAGE			
unclassified	**unclassified**	**unclassified**	**Same as Report (SAR)**	**33**	

subject to the constraints

$$\nabla \cdot E = 0 = \nabla \cdot B. \tag{1.3}$$

The constraints (1.3) are clearly preserved under the time evolution governed by (1.1)–(1.2).

Our problem is to specify radiation boundary conditions at an artificial boundary $\Gamma \subset \partial\Omega$ so that the solution computed in Ω can be made arbitrarily close to the restriction to Ω of the solution of the original problem on the unbounded domain. We will organize the discussion around four general classes of methods: fast methods based on separation of variables on symmetric boundaries, methods for general boundaries beased on the retarded potential, methods based on equivalent source representations, and, finally, convergent local approximations. We note that there have been parallel developments for other applications and refer the reader to [35, 36] for more comprehensive if slightly older reviews.

2. Boundaries with symmetry

For plane, spherical, and cylindrical boundaries, this section formulates exact nonreflecting boundary conditions for the homogeneous Maxwell equations. An earlier review article [35] described these boundary conditions from a more general perspective. In contrast, our presentation here considers only the Maxwell system (1.1)–(1.2) and derives the relevant boundary conditions and effective numerical approximations from the ground up.

2.1. **Planar boundary.**

Let $x_1 = x = 0$ specify the planar boundary of the "computational domain" $x < 0$. On the system (1.1)–(1.2) we perform both a Laplace transform (denoted by a hat) in time and a Fourier transform (denoted by a bar) in the tangential variables $(x_2, x_3) = (y, z)$, thereby obtaining a differential–algebraic system. With (k_2, k_3) representing the Fourier variables dual to (y, z), the system's algebraic sector is

$$\tilde{s}\hat{\bar{E}}_1 = ik_2\hat{\bar{B}}_3 - ik_3\hat{\bar{B}}_2, \qquad \tilde{s}\hat{\bar{B}}_1 = -ik_2\hat{\bar{E}}_3 + ik_3\hat{\bar{E}}_2, \tag{2.4}$$

where $\tilde{s} = s/c$. Using these algebraic equations, we may then express the remaining differential sector solely in terms of the tangential variables as follows:

$$\frac{\partial}{\partial x}\begin{pmatrix} \hat{\bar{E}}_2 \\ \hat{\bar{E}}_3 \\ \hat{\bar{B}}_2 \\ \hat{\bar{B}}_3 \end{pmatrix} = \begin{pmatrix} 0 & 0 & \frac{k_2k_3}{\tilde{s}} & -\frac{(\tilde{s}^2+k_2^2)}{\tilde{s}} \\ 0 & 0 & \frac{(\tilde{s}^2+k_3^2)}{\tilde{s}} & -\frac{k_2k_3}{\tilde{s}} \\ -\frac{k_2k_3}{\tilde{s}} & \frac{(\tilde{s}^2+k_2^2)}{\tilde{s}} & 0 & 0 \\ -\frac{(\tilde{s}^2+k_3^2)}{\tilde{s}} & \frac{k_2k_3}{\tilde{s}} & 0 & 0 \end{pmatrix}\begin{pmatrix} \hat{\bar{E}}_2 \\ \hat{\bar{E}}_3 \\ \hat{\bar{B}}_2 \\ \hat{\bar{B}}_3 \end{pmatrix}. \tag{2.5}$$

The eigenvalues of the matrix are

$$\lambda_\pm = \pm\sqrt{\tilde{s}^2 + k_2^2 + k_3^2} = \pm\sqrt{\tilde{s}^2 + |k|^2}, \tag{2.6}$$

with each one doubly degenerate. In (2.6) we define the branch to ensure that λ_+ has positive real part for $\mathrm{Re}\tilde{s} > 0$, and $\lambda_+ \sim \tilde{s}$ as $\tilde{s} \to \infty$. As the branch cut we choose a curve in the left–half $\tilde{s}$–plane running from $i|k|$ to $-i|k|$. Our radiation conditions demand that solutions to (2.5) remain bounded as $x \to \infty$.

Such solutions are then of the form

(2.7)
$$e^{-x\sqrt{\tilde{s}^2+|k|^2}}\left\{a(\tilde{s},k_2,k_3)\begin{pmatrix}\tilde{s}^2+k_2^2\\ k_2k_3\\ 0\\ \tilde{s}\sqrt{\tilde{s}^2+|k|^2}\end{pmatrix}+b(\tilde{s},k_2,k_3)\begin{pmatrix}-k_2k_3\\ -\tilde{s}^2-k_3^2\\ \tilde{s}\sqrt{\tilde{s}^2+|k|^2}\\ 0\end{pmatrix}\right\}.$$

Straightforward calculations show that for this subspace the solution components obey the relationships

(2.8)
$$\left[\sqrt{\tilde{s}^2+|k|^2}+\tilde{s}+\frac{k_3^2}{\tilde{s}}\right]\hat{\tilde{E}}_2-\frac{k_2k_3}{\tilde{s}}\hat{\tilde{E}}_3+\frac{k_2k_3}{\tilde{s}}\hat{\tilde{B}}_2-\left[\sqrt{\tilde{s}^2+|k|^2}+\tilde{s}+\frac{k_2^2}{\tilde{s}}\right]\hat{\tilde{B}}_3=0,$$

(2.9)
$$-\frac{k_2k_3}{\tilde{s}}\hat{\tilde{E}}_2+\left[\sqrt{\tilde{s}^2+|k|^2}+\tilde{s}+\frac{k_2^2}{\tilde{s}}\right]\hat{\tilde{E}}_3+\left[\sqrt{\tilde{s}^2+|k|^2}+\tilde{s}+\frac{k_3^2}{\tilde{s}}\right]\hat{\tilde{B}}_2-\frac{k_2k_3}{\tilde{s}}\hat{\tilde{B}}_3=0.$$

The earlier review article [35] discusses the origin of these relationships in terms of the left eigenvectors of the matrix appearing in (2.5).

To produce physical–space time–domain radiation conditions from (2.8)–(2.9), we must carry out the necessary inverse transformations. We first introduce the kernel [35, 3]

$$K(t)=t^{-1}J_1(t),\quad \hat{K}(s)=\sqrt{s^2+1}-s, \tag{2.10}$$

where of course $\hat{K}(s)$ decays in s. In (2.8)–(2.9) we set

$$\sqrt{\tilde{s}^2+|k|^2}+\tilde{s}=|k|\hat{K}\big(|k|^{-1}\tilde{s}\big)+2\tilde{s}, \tag{2.11}$$

rearrange terms, and make substitutions with (2.4), in order to reach a set of equations on which the inverse transformations are easily carried out. We then find

$$\frac{2}{c}\frac{\partial}{\partial t}(E_2-B_3)+\mathcal{R}(E_2-B_3)+\frac{\partial E_1}{\partial y}-\frac{\partial B_1}{\partial z}=0, \tag{2.12}$$

$$\frac{2}{c}\frac{\partial}{\partial t}(E_3+B_2)+\mathcal{R}(E_3+B_2)+\frac{\partial E_1}{\partial z}+\frac{\partial B_1}{\partial y}=0, \tag{2.13}$$

where the nonlocal operation $(\mathcal{R}w)(0,y,z,t)$ is defined through

$$\mathcal{F}\big(\mathcal{R}w\big)(0,k_2,k_3,t)=\int_0^t\frac{J_1\big(c|k|\tau\big)}{c|k|\tau}\left[c|k|^2\bar{w}(0,k_2,k_3,t-\tau)\right]d\tau. \tag{2.14}$$

Here $\mathcal{F}$ denotes Fourier transform in the tangential variables (y,z), and succinctly

$$\mathcal{R}w=\mathcal{F}^{-1}\big(c|k|^2K(c|k|t)*(\mathcal{F}w)\big). \tag{2.15}$$

We note that analogous expressions can be derived in waveguides, which is the most practical application of the planar boundary formulas. We consider only the simplest possible case. In particular, suppose that for $x>0$ the waveguide has constant rectangular cross-section, $\Theta=[0,L_y]\times[0,L_z]$. Suppose further that the walls are perfectly conducting. Then we may replace the Fourier transfroms in the expressions above by Fourier series. (Note that for more complicated cross-sections the relevant eigenfunction expansions couple Cartesian components in a nontrivial way.) Noting the boundary conditions and divergence constraint we conclude that E_2 and B_3 should be expanded in terms of $\cos\left(\frac{k_2\pi y}{L_y}\right)\cdot\sin\left(\frac{k_3\pi z}{L_z}\right)\equiv CS_{k_2,k_3}$ while

E_3 and B_2 are expressed in terms of $\sin\left(\frac{k_2\pi y}{L_y}\right)\cdot\cos\left(\frac{k_3\pi z}{L_z}\right)\equiv SC_{k_2,k_3}$. (See, e.g, [61, Ch. 9].) We must now only replace $\mathcal{F}$ by the series transform $\mathcal{F}_{CS}$ in equation (2.12) and $\mathcal{F}_{SC}$ in equation (2.13), noting that now $|k|^2=\pi^2\left(\frac{k_2^2}{L_y^2}+\frac{k_3^2}{L_z^2}\right)$.

Refs. [3, 50] present efficient strategies for numerically implementing the convolution (2.15), and these methods will be discussed below. Such approximations obviate the need to carry out the exact inverse Fourier transform in (2.15). Nevertheless, as an interesting exercise we here perform this inverse transformation in order to achieve the exact physical–space time–domain boundary conditions. First, with $\mathbf{y}=(y,z)$, $\mathbf{k}=(k_2,k_3)$, $\mathbf{u}=(u,v)$, and

$$F(k_2,k_3)=\frac{1}{2\pi}\int_{\mathbb{R}^2}e^{-i\mathbf{y}\cdot\mathbf{k}}f(y,z)d\mathbf{y},\quad f(y,z)=\frac{1}{2\pi}\int_{\mathbb{R}^2}e^{i\mathbf{y}\cdot\mathbf{k}}F(k_2,k_3)d\mathbf{k}, \tag{2.16}$$

recall that by the Fourier convolution theorem

$$\mathcal{F}^{-1}\big[F(k_2,k_3)G(k_2,k_3)\big](y,z)=\frac{1}{2\pi}\int_{\mathbb{R}^2}f(y-u,z-v)g(u,v)d\mathbf{u}. \tag{2.17}$$

In order to apply the convolution theorem (2.17), we first assemble several results from Watson's monograph [74] in order to compute the inverse Fourier transform

$$\frac{1}{2\pi}\int_{\mathbb{R}^2}e^{i\mathbf{y}\cdot\mathbf{k}}\frac{J_1(c|k|t)}{c|k|t}d\mathbf{k}=\frac{H(t-\rho/c)}{c^2t^2}, \tag{2.18}$$

where $\rho=\sqrt{y^2+z^2}$ and $H(\xi)$ is the Heaviside step function such that $H(\xi)=0$ for $\xi<0$, $H(0)=\frac{1}{2}$, $H(\xi)=1$ for $\xi>0$. With these results, we find that

$$(\mathcal{R}w)(0,y,z,t)=-\frac{1}{2\pi}\int_0^t\frac{1}{c(t-\tau)^2}\int_{|\mathbf{y}-\mathbf{u}|\le c(t-\tau)}\Delta_{\mathbf{u}}w(0,u,v,\tau)d\mathbf{u}d\tau, \tag{2.19}$$

with $\Delta_{\mathbf{u}}$ denoting the Laplacian in the u–v plane. The divergence theorem then gives

$$(\mathcal{R}w)(0,y,z,t)= \\ -\frac{1}{2\pi}\int_0^t\frac{1}{c(t-\tau)}\frac{\partial}{\partial t}\int_0^{2\pi}w(0,y+c(t-\tau)\cos\theta,z+c(t-\tau)\sin\theta,\tau)d\theta d\tau. \tag{2.20}$$

Notice that the integration is over the intersection of the artificial boundary $x=0$ and the past lightcone belonging to the spacetime point $(0,y,z,t)$.

2.2. **Spherical boundary.**

2.2.1. *Vector spherical harmonics.* We consider both *pure–spin* and *pure–orbital* vector spherical harmonics (see [69] for the origins of this terminology). As given in [35, 53, 56, 55], the unnormalized pure–spin harmonics are the set

$$\begin{aligned}\mathbf{Y}_{\ell m}=&Y_{\ell m}\mathbf{e}_r,\\ \mathbf{\Psi}_{\ell m}=&\frac{\partial Y_{\ell m}}{\partial\theta}\mathbf{e}_\theta+\frac{1}{\sin\theta}\frac{\partial Y_{\ell m}}{\partial\phi}\mathbf{e}_\phi,\\ \mathbf{\Phi}_{\ell m}=&-\frac{1}{\sin\theta}\frac{\partial Y_{\ell m}}{\partial\phi}\mathbf{e}_\theta+\frac{\partial Y_{\ell m}}{\partial\theta}\mathbf{e}_\phi,\end{aligned} \tag{2.21}$$

where $\mathbf{e}_r$, $\mathbf{e}_\theta$, and $\mathbf{e}_\phi$ are the standard unit basis vectors in the spherical polar coordinate system and

$$Y_{\ell m}(\theta,\phi) = \sqrt{\frac{2\ell+1}{4\pi}\frac{(\ell-m)!}{(\ell+m)!}}e^{im\phi}P_\ell^m(\cos\theta), \tag{2.22}$$

is one of the standard spherical harmonics, orthogonal on the unit sphere. (Here P_ℓ^m is the associated Legendre function defined in [1], Ch. 8.) When paired with r–dependent expansion coefficients, these harmonics are easily seen to form a closed system under the standard vector operations (div, grad, curl) involving the gradient operator ∇ [55]. In terms of the pure–spin harmonics, we also define a set of normalized pure–orbital vector harmonics,

$$\begin{aligned}
\mathbf{W}_{\ell m} =& \mathbf{Y}^{\ell-1}_{\ell m} = \sqrt{\frac{\ell+1}{2\ell+1}}\left[\frac{1}{\sqrt{\ell(\ell+1)}}\mathbf{\Psi}_{\ell m}\right] + \sqrt{\frac{\ell}{2\ell+1}}\mathbf{Y}_{\ell m},\\
\mathbf{X}_{\ell m} =& \mathbf{Y}^{\ell}_{\ell m} = -i\left[\frac{1}{\sqrt{\ell(\ell+1)}}\mathbf{\Phi}_{\ell m}\right],\\
\mathbf{V}_{\ell m} =& \mathbf{Y}^{\ell+1}_{\ell m} = \sqrt{\frac{\ell}{2\ell+1}}\left[\frac{1}{\sqrt{\ell(\ell+1)}}\mathbf{\Psi}_{\ell m}\right] - \sqrt{\frac{\ell+1}{2\ell+1}}\mathbf{Y}_{\ell m}.
\end{aligned} \tag{2.23}$$

The $\mathbf{Y}^{\ell'}_{\ell m}$ are Thorne's $\mathbf{Y}^{\ell',\ell m}$ [69], and the $\mathbf{V}_{\ell m}$, $\mathbf{X}_{\ell m}$, $\mathbf{W}_{\ell m}$ notation is due to Hill [47]. When paired with r–dependent expansion coefficients, the pure–orbital harmonics also form a closed system under the standard vector operations involving the gradient operator ∇, and a compendium of formulas is given by Hill [47]. Apart from the factors of $1/\sqrt{\ell(\ell+1)}$, which serve to normalize the pure–spin harmonics (2.21), the matrix associated with the transformation (2.23) is unitary.

The orbital harmonics (2.23) also arise in the quantum theory of angular momenta [11]. Indeed, in terms of the complexified basis $\mathbf{t}_0 = \mathbf{e}_z$, $\mathbf{t}_{\pm1} = \mp(\mathbf{e}_x \pm i\mathbf{e}_y)/\sqrt{2}$, they are

$$\mathbf{Y}^{\ell'}_{\ell m} = \sum_{m'=-\ell'}^{\ell'}\sum_{m''=-1}^{1}(\ell' 1 m' m''|\ell' 1 \ell m) Y_{\ell' m'}\mathbf{t}_{m''}, \tag{2.24}$$

where the $(\ell' 1 m' m''|\ell' 1 \ell m)$ are Clebsch–Gordan coefficients [1, 11]. For fixed ℓ the $\mathbf{Y}^{\ell'}_{\ell m}$ transform under an order–ℓ representation of the rotation group $SO(3)$. The expansion above expresses this representation as a coupling between the scalar harmonics $Y_{\ell',m}$ (an order–ℓ' representation, where $\ell' = \ell-1, \ell, \ell+1$) and the basis $\mathbf{t}_m$ (an order–1 representation). Starting from (2.23) and using identities for the scalar harmonics (collected, for example, in [48]), one may also directly calculate the following explicit expressions:

$$\begin{aligned}
\mathbf{Y}^{\ell-1}_{\ell m} =& \sqrt{\frac{(\ell+m)(\ell+m-1)}{2\ell(2\ell-1)}}Y_{\ell-1,m-1}\mathbf{t}_1\\
&+\sqrt{\frac{(\ell-m)(\ell+m)}{\ell(2\ell-1)}}Y_{\ell-1,m}\mathbf{t}_0\\
&+\sqrt{\frac{(\ell-m)(\ell-m-1)}{2\ell(2\ell-1)}}Y_{\ell-1,m+1}\mathbf{t}_{-1},
\end{aligned}$$

$$\begin{aligned}\mathbf{Y}^{\ell}_{\ell m} =& -\sqrt{\frac{(\ell+m)(\ell-m+1)}{2\ell(\ell+1)}}Y_{\ell,m-1}\mathbf{t}_1\\ &+m\sqrt{\frac{1}{\ell(\ell+1)}}Y_{\ell,m}\mathbf{t}_0\\ &+\sqrt{\frac{(\ell-m)(\ell+m+1)}{2\ell(\ell+1)}}Y_{\ell,m+1}\mathbf{t}_{-1},\end{aligned} \tag{2.25}$$

$$\begin{aligned}\mathbf{Y}^{\ell+1}_{\ell m} =&\sqrt{\frac{(\ell-m+1)(\ell-m+2)}{(2\ell+2)(2\ell+3)}}Y_{\ell+1,m-1}\mathbf{t}_1\\ &-\sqrt{\frac{(\ell+m+1)(\ell-m+1)}{(\ell+1)(2\ell+3)}}Y_{\ell+1,m}\mathbf{t}_0\\ &+\sqrt{\frac{(\ell+m+1)(\ell+m+2)}{(2\ell+2)(2\ell+3)}}Y_{\ell+1,m+1}\mathbf{t}_{-1}.\end{aligned}$$

The factors involving square roots are the nonzero Clebsch–Gordan coefficients in the expansion (2.24). Unlike the pure–spin harmonics (2.21), the $\mathbf{Y}^{\ell'}_{\ell m}$ are eigenfunctions of the spherical Laplacian with eigenvalue $-\ell'(\ell'+1)$.

2.2.2. *Exact radiation boundary conditions.* Using the pure–spin harmonics, Ref. [35] has formulated exact radiation boundary conditions for the electromagnetic field in the presence of a spherical boundary. Here we will provide an equivalent description in terms of the pure–orbital harmonics. Nevertheless, since they are tailored to the transverse character of the radiation field, we at first work with the pure–spin harmonics, only converting to the pure–orbital harmonics once our calculations have been completed.

To start, we perform a Laplace transform on the system (1.1)–(1.2), subsequently expanding the transformed variables $\hat{E}$ and $\hat{B}$ in pure–spin harmonics. The $\hat{E}$ expansion, for example, is

$$\hat{E} = \sum_{\ell=1}^{\infty}\sum_{m=-\ell}^{\ell}\left[\hat{E}^r_{\ell m}\mathbf{Y}_{\ell m} + \hat{E}^{(1)}_{\ell m}\mathbf{\Psi}_{\ell m} + \hat{E}^{(2)}_{\ell m}\mathbf{\Phi}_{\ell m}\right]. \tag{2.26}$$

This process leads to a differential–algebraic system of equations, where the algebraic sector is

$$\tilde{s}\hat{E}^r_{\ell m} = -\frac{\ell(\ell+1)}{r}\hat{B}^{(2)}_{\ell m}, \quad \tilde{s}\hat{B}^r_{\ell m} = \frac{\ell(\ell+1)}{r}\hat{E}^{(2)}_{\ell m}. \tag{2.27}$$

These equations may be used to eliminate the radial–harmonic coefficients, $\hat{E}^r_{\ell m}$ and $\hat{B}^r_{\ell m}$, and such an elimination yields the following first–order system for the remaining coefficients:

$$\left(\frac{\partial}{\partial r}+\frac{1}{r}\right)\begin{pmatrix}\hat{E}^{(1)}_{\ell m}\\ \hat{E}^{(2)}_{\ell m}\\ \hat{B}^{(1)}_{\ell m}\\ \hat{B}^{(2)}_{\ell m}\end{pmatrix} = \tilde{s}\begin{pmatrix}0 & 0 & 0 & -1-\frac{\ell(\ell+1)}{\tilde{s}^2r^2}\\ 0 & 0 & 1 & 0\\ 0 & 1+\frac{\ell(\ell+1)}{\tilde{s}^2r^2} & 0 & 0\\ -1 & 0 & 0 & 0\end{pmatrix}\begin{pmatrix}\hat{E}^{(1)}_{\ell m}\\ \hat{E}^{(2)}_{\ell m}\\ \hat{B}^{(1)}_{\ell m}\\ \hat{B}^{(2)}_{\ell m}\end{pmatrix}. \tag{2.28}$$

The solutions

$$a_{\ell m}(\tilde{s})\begin{pmatrix} k'_\ell(\tilde{s}r)+\frac{k_\ell(\tilde{s}r)}{\tilde{s}r} \\ 0 \\ 0 \\ -k_\ell(\tilde{s}r)\end{pmatrix} + b_{\ell m}(\tilde{s})\begin{pmatrix} 0 \\ k_\ell(\tilde{s}r) \\ k'_\ell(\tilde{s}r)+\frac{k_\ell(\tilde{s}r)}{\tilde{s}r} \\ 0\end{pmatrix} \tag{2.29}$$

remain finite as $r \to \infty$ for $\mathrm{Re}(\tilde{s}) > 0$. Here $k_\ell(z)$ is a modified spherical Bessel function expressed as $k_\ell(z) = \sqrt{\pi/(2z)}K_{\ell+1/2}(z)$ in terms of the standard modified cylindrical Bessel function $K_\nu(z)$ known as the MacDonald function [74]. As defined,

$$k_\ell(z) \sim \pi(2z)^{-1}e^{-z} \quad \text{as} \quad z \to \infty, \tag{2.30}$$

but some authors fix the definition of $k_\ell(z)$ so that $k_\ell(z) \sim z^{-1}e^{-z}$. In any case, the choice of the overall of overall constant does not affect our argument. From now on we assume that the multipole components have the stated form, so, for example, $\hat{B}^{(2)}_{\ell m} = -a_{\ell m}(\tilde{s})k_\ell(\tilde{s}r)$. Further calculations then show that

$$\tilde{s}\big(\hat{E}^{(2)}_{\ell m}+\hat{B}^{(1)}_{\ell m}\big)+\frac{1}{r}\hat{M}_\ell(\tilde{s}r)\hat{E}^{(2)}_{\ell m}=0, \qquad \tilde{s}\big(\hat{E}^{(1)}_{\ell m}-\hat{B}^{(2)}_{\ell m}\big)-\frac{1}{r}\hat{M}_\ell(\tilde{s}r)\hat{B}^{(2)}_{\ell m}=0. \tag{2.31}$$

Here the frequency-domain kernel is

$$\hat{M}_\ell(z) = -\left[1+z+z\frac{k'_\ell(z)}{k_\ell(z)}\right] = -\left[\frac{1}{2}+z+z\frac{K'_{\ell+1/2}(z)}{K_{\ell+1/2}(z)}\right]. \tag{2.32}$$

In fact $\hat{M}_\ell(z) = O(1/z)$, so that overall $r^{-1}\hat{M}_\ell(\tilde{s}r)$ is $O(1/r^2)$ in the radial coordinate.

By the Laplace convolution theorem, the corresponding time–domain boundary conditions are then (with $r = R$ taken as the boundary location)

$$\frac{1}{c}\frac{\partial}{\partial t}\big(E^{(2)}_{\ell m}+B^{(1)}_{\ell m}\big)+\frac{1}{R}\int_0^t M_\ell(c\tau/R)E^{(2)}_{\ell m}(R,t-\tau)d\tau=0, \tag{2.33}$$

$$\frac{1}{c}\frac{\partial}{\partial t}\big(E^{(1)}_{\ell m}-B^{(2)}_{\ell m}\big)-\frac{1}{R}\int_0^t M_\ell(c\tau/R)B^{(2)}_{\ell m}(R,t-\tau)d\tau=0, \tag{2.34}$$

where the time–domain kernel is

$$M_\ell(ct/R) = -\sum_{k=1}^{\ell}(z_{\ell,k}/R)\exp(z_{\ell,k}ct/R) \tag{2.35}$$

in terms of the ℓ roots $z_{\ell,k}$ of $K_{\ell+1/2}(z)$ which all lie in the left–half plane z–plane.

As will be discussed in subsequent sections, the fact that the kernels are exponential functions of t implies that the temporal convolution can be **localized**. That is, one can avoid the storage of the time history evident in (2.33)-(2.34). This fact was independently exploited by Sofronov [63, 64] and Grote and Keller [28, 29, 30] to derive and implement accurate temporally local conditions. (See also [31] for applications to multiple scattering.) In fact, in [38] it is shown that purely local conditions can be developed which are exact for solutions described by finitely many spherical harmonics. In particular, setting $w_0 = 2u$, $w_{P+1} = 0$ and solving the following coupled sequence of equations on the sphere:

$$\frac{1}{c}\frac{\partial w_j}{\partial t}+\frac{j}{R}w_j = \frac{1}{4R^2}\left(\Delta_{S^2}+j(j-1)\right)w_{j-1}+w_{j+1}, \quad j=1,\ldots,P, \tag{2.36}$$

it is shown that:

$$w_1 + \frac{1}{R}\sum_{\ell=0}^{P}\sum_{m=-\ell}^{\ell} Y_{\ell m}\left(M_\ell * u_{\ell m}\right) = 0, \tag{2.37}$$

if we assume $u_{\ell m} = 0$ for $\ell > P$. This local exact condition has been successfully implemented by Grote [27].

These formulations become expensive as the harmonic index, ℓ, increases as (2.35) requires ℓ exponentials. However, as described in [2], for large ℓ one may use compressed kernels and fewer exponential terms while retaining high accuracy. We will describe this development below.

Introducing $\bar{B} = \mathbf{e}_r \times B = -B_\phi \mathbf{e}_\theta + B_\theta \mathbf{e}_\phi$, so that $B^{(1)}_{\ell m} = \bar{B}^{(2)}_{\ell m}$ and $-B^{(2)}_{\ell m} = \bar{B}^{(1)}_{\ell m}$, we then write (2.33)–(2.34) as follows:

$$\frac{1}{c}\frac{\partial}{\partial t}\big(E^{(2)}_{\ell m} + \bar{B}^{(2)}_{\ell m}\big) + \frac{1}{R}\big(M_\ell * E^{(2)}_{\ell m}\big) = 0 \tag{2.38}$$

$$\frac{1}{c}\frac{\partial}{\partial t}\big(E^{(1)}_{\ell m} + \bar{B}^{(1)}_{\ell m}\big) + \frac{1}{R}\big(M_\ell * \bar{B}^{(1)}_{\ell m}\big) = 0. \tag{2.39}$$

Finally, summing these equations on the harmonics, we obtain

$$\frac{1}{c}\frac{\partial}{\partial t}\big(E^T + \bar{B}\big) + \frac{1}{R}\sum_{\ell=1}^{\infty}\sum_{m=-\ell}^{\ell}\left[\mathbf{\Psi}_{\ell m}\big(M_\ell * \bar{B}^{(1)}_{\ell m}\big) + \mathbf{\Phi}_{\ell m}\big(M_\ell * E^{(2)}_{\ell m}\big)\right], \tag{2.40}$$

where the superscript T denotes "transverse", that is $E^T = E - E(E \cdot \mathbf{e}_r)$. Note that $E^T + B$ has components $(0, E_\theta - B_\phi, E_\theta + B_\phi)$.

We now rewrite (2.40) in terms of the pure–orbital harmonics, thereby achieving an expression which may be implemented using the scalar–harmonic transform. Since $\bar{B} = \bar{B}^T$, it follows from (2.23) that

$$\bar{B}^{(\ell-1)}_{\ell m} = \sqrt{\frac{\ell}{2\ell+1}}(\ell+1)\bar{B}^{(1)}_{\ell m}, \quad \bar{B}^{(\ell+1)}_{\ell m} = \sqrt{\frac{\ell+1}{2\ell+1}}\ell\bar{B}^{(1)}_{\ell m}. \tag{2.41}$$

Here the expansion coefficients are with respect the pure–orbital harmonics,

$$\bar{B}^{(\ell')}_{\ell m} = \int_{S^2} \bar{B}\cdot\overline{\mathbf{Y}}^{\ell'}_{\ell m} dS, \tag{2.42}$$

where the overline on $\overline{\mathbf{Y}}$ indicates complex conjugation and dS is the area measure on the unit sphere S^2. In terms of the pure–orbital harmonics, the boundary condition (2.40) becomes

$$\begin{aligned} 0 = &\frac{1}{c}\frac{\partial}{\partial t}\big(E^T + \bar{B}\big) + \\ &\frac{1}{R}\sum_{\ell=1}^{\infty}\sum_{m=-\ell}^{\ell}\left[\mathbf{Y}^{\ell-1}_{\ell m}\big(M_\ell * \bar{B}^{(\ell-1)}_{\ell m}\big) + \mathbf{Y}^{\ell+1}_{\ell m}\big(M_\ell * \bar{B}^{(\ell+1)}_{\ell m}\big) + \mathbf{Y}^{\ell}_{\ell m}\big(M_\ell * E^{(\ell)}_{\ell m}\big)\right]. \end{aligned} \tag{2.43}$$

Taking advantage of the list (2.25), we may use the scalar–harmonic transform to compute the coefficients $\bar{B}^{(\ell')}_{\ell m}$ and $E^{(\ell')}_{\ell m}$. This fact is significant for practical implementations as we can use well-developed software for computing and inverting the transform. (See, for example, the routines distributed with the NCAR spectral transform shallow water model [57].)

2.3. **Cylindrical boundary.** Our last example is a cylindrical boundary of infinite extent, defined in terms of the standard cylindrical coordinate system (r, θ, z) as $r = R$. We expand the vector field E in terms of the standard orthonormal cylindrical basis $\{\mathbf{e}_r, \mathbf{e}_\theta, \mathbf{e}_z\}$ as $E = E_r\mathbf{e}_r + E_\theta\mathbf{e}_\theta + E_z\mathbf{e}_z$, and similarly for B. Next, we write down the Maxwell system (1.1)–(1.2) component–by–component, subsequently performing on each field component a Laplace transform in t (with dual variable s and denoted by a hat), continuous Fourier transform in z (with dual variable k and denoted by a bar), and a Fourier series expansion in θ (with dual index n and denoted by a superscript n). Like before, this process yields both algebraic equations,

$$\tilde{s}\hat{\bar{E}}_r^n - \left(\frac{in}{r}\hat{\bar{B}}_z^n - ik\hat{\bar{B}}_\theta^n\right) = 0, \quad \tilde{s}\hat{\bar{B}}_r^n + \left(\frac{in}{r}\hat{\bar{E}}_z^n - ik\hat{\bar{E}}_\theta^n\right) = 0, \tag{2.44}$$

as well as a system of ordinary differential equations,

$$\frac{\partial}{\partial r}\begin{pmatrix} r\hat{\bar{E}}_\theta^n \\ \hat{\bar{E}}_z^n \\ r\hat{\bar{B}}_\theta^n \\ \hat{\bar{B}}_z^n \end{pmatrix} + \begin{pmatrix} 0 & 0 & -\frac{kn}{\tilde{s}r} & \tilde{s}r + \frac{n^2}{\tilde{s}r} \\ 0 & 0 & -\frac{\tilde{s}}{r} - \frac{k^2}{\tilde{s}r} & \frac{kn}{\tilde{s}r} \\ \frac{kn}{\tilde{s}r} & -\tilde{s}r - \frac{n^2}{\tilde{s}r} & 0 & 0 \\ \frac{\tilde{s}}{r} + \frac{k^2}{\tilde{s}r} & -\frac{kn}{\tilde{s}r} & 0 & 0 \end{pmatrix}\begin{pmatrix} r\hat{\bar{E}}_\theta^n \\ \hat{\bar{E}}_z^n \\ r\hat{\bar{B}}_\theta^n \\ \hat{\bar{B}}_z^n \end{pmatrix} = 0. \tag{2.45}$$

The solutions which remain finite as $r \to \infty$ have the form

$$\begin{pmatrix} r\hat{\bar{E}}_\theta^n \\ \hat{\bar{E}}_z^n \\ r\hat{\bar{B}}_\theta^n \\ \hat{\bar{B}}_z^n \end{pmatrix} = a_n(\tilde{s}, k)\begin{pmatrix} \frac{kn}{\sigma^2}K_n(r\sigma) \\ K_n(r\sigma) \\ \frac{\tilde{s}r}{\sigma}K_n'(r\sigma) \\ 0 \end{pmatrix} + b_n(\tilde{s}, k)\begin{pmatrix} -\frac{\tilde{s}r}{\sigma}K_n'(r\sigma) \\ 0 \\ \frac{kn}{\sigma^2}K_n(r\sigma) \\ K_n(r\sigma) \end{pmatrix}, \tag{2.46}$$

where $\sigma = \sqrt{\tilde{s}^2 + k^2}$, with the branch chosen as in plane boundary example. Notice that $\sigma - \tilde{s} = k\hat{K}(k^{-1}\tilde{s})$, where the kernel $\hat{K}(s)$, first appearing in (2.10), should not be confused with the MacDonald function $K_n(r\sigma)$. For the chosen subspace (2.46) of solutions the components satisfy the relationships

$$\tilde{s}\big(\hat{\bar{E}}_z^n + \hat{\bar{B}}_\theta^n\big) + \frac{\hat{\bar{E}}_z^n}{2r} + ik\hat{\bar{E}}_r^n + k\hat{K}(k^{-1}\tilde{s})\hat{\bar{E}}_z^n + \frac{1}{r}\hat{C}_n\big(r\sqrt{\tilde{s}^2 + k^2}\big)\hat{\bar{E}}_z^n = 0, \tag{2.47}$$

$$\tilde{s}\big(\hat{\bar{B}}_z^n - \hat{\bar{E}}_\theta^n\big) + \frac{\hat{\bar{B}}_z^n}{2r} + ik\hat{\bar{B}}_r^n + k\hat{K}(k^{-1}\tilde{s})\hat{\bar{B}}_z^n + \frac{1}{r}\hat{C}_n\big(r\sqrt{\tilde{s}^2 + k^2}\big)\hat{\bar{B}}_z^n = 0. \tag{2.48}$$

To reach these equations we have made use of (2.44) and introduced

$$\hat{C}_n(z) = -\left[\frac{1}{2} + z + z\frac{K_n'(z)}{K_n(z)}\right]. \tag{2.49}$$

Since $\hat{C}_n(z) \sim z^{-1}$ as $z \to \infty$, the kernel $\hat{C}_n\big(r\sqrt{\tilde{s}^2 + k^2}\big)$ is the Laplace transform of a function $G_n(ct, r, k)$. We may now easily perform the requisite inverse transformations on (2.47)–(2.48). Evaluated at the boundary $r = R$, the results are

$$\frac{1}{c}\frac{\partial}{\partial t}\big(E_z + B_\theta\big) + \frac{E_z}{2R} + \frac{\partial E_r}{\partial z} + \mathcal{R}_z E_z + \mathcal{Q}_{\theta z}E_z = 0, \tag{2.50}$$

$$\frac{1}{c}\frac{\partial}{\partial t}\big(B_z - E_\theta\big) + \frac{B_z}{2R} + \frac{\partial B_r}{\partial z} + \mathcal{R}_z B_z + \mathcal{Q}_{\theta z}B_z = 0. \tag{2.51}$$

Here, with $\mathcal{F}_z$ indicating Fourier transform in z and $w = w(R, \theta, z, t)$, we define

$$\mathcal{R}_z w = \mathcal{F}_z^{-1}\big(ck^2 K(ckt) * (\mathcal{F}_z w)\big), \tag{2.52}$$

which is similar to formula (2.15). Moreover, with $\mathcal{F}_{\theta z}$ representing double Fourier transformation in θ (series) and z (continuous), the remaining nonlocal operation is

$$\mathcal{Q}_{\theta z} w = \mathcal{F}_{\theta z}^{-1}\big(G_n(ct, R, k) * \mathcal{F}_{\theta z} w\big). \tag{2.53}$$

Although we will not explicitly perform the inverse Laplace and Fourier transforms in order to define the exact time–domain physical–space boundary conditions, we note that efficient strategies exist for numerically implementing these nonlocal operations [3].

2.4. **Fast time-local evaluation of the kernels I: global exponential approximations.** Clearly, a primary bottleneck in the direct evaluation of the exact boundary conditions derived above is the evaluation of integral operators. To give a rough count of the complexity, we suppose lengths are scaled by the dimensions of the computational domain, and time is scaled so that $c = 1$. Then the integration time, T, measures the number of times a wave could traverse the domain. If a characteristic wavelength in these units is given by λ the complexity of a standard solver would be:

$$\text{Work} \propto \lambda^{-4} T, \quad \text{Storage} \propto \lambda^{-3}. \tag{2.54}$$

A reasonable goal is that the cost of boundary treatment is no worse than these. Specializing to the spherical boundary, the cost per time step associated with the integrals is the sum of the cost of the spherical harmonic transform and the cost of the temporal convolution. Noting that the number of harmonics required will scale like λ^{-2}, the use of standard software such as [57], which combines FFTs in the azimuthal coordinate with direct transforms in θ, leads to a total cost of:

$$\text{Work}_{\text{SHT}} \propto \lambda^{-4} T, \tag{2.55}$$

which is comparable to (and in practice less than) the work required by the volume solver. For $\lambda \ll 1$ one could instead use one of the recently developed fast spherical harmonic transforms (e.g. [52, 43, 65]). These reduce the complexity to:

$$\text{Work}_{\text{SHT}} \propto \lambda^{-3} \ln(\lambda^{-1}) T. \tag{2.56}$$

The work associated with the temporal convolution can also be kept manageable through the use of fast alogrithms. Precisely, Hairer et al [41] show that the well-known FFT-based algorithms for computing convolutions can be adapted to evolutional convolution integrals of our form. Using their algorithm we have:

$$\text{Work}_{\text{conv}} \propto \lambda^{-3} \ln^2(\lambda^{-1}) T \ln^2 T. \tag{2.57}$$

However, the algorithm in [41] requires full storage of the boundary history:

$$\text{Storage}_{\text{conv}} \propto \lambda^{-3} T. \tag{2.58}$$

This is the dominant storage cost for T large, and is prohibitive for large applications.

The key idea in developing fast, low-storage implementations of the exact boundary conditions is the observation that convolution with exponential functions requires no history storage. Precisely, if:

$$\phi(t) = \int_0^t \alpha e^{\beta(t-\tau)} u(\tau) d\tau, \tag{2.59}$$

then ϕ satisfies the differential equation:

$$\frac{d\phi}{dt} = \beta\phi + \alpha u. \tag{2.60}$$

We can thus expect to compute ϕ using $O(\lambda^{-1}T)$ work and $O(1)$ storage, vastly improving on the general algorithm of [41]. For the case of a spherical boundary, we have already observed that the kernels are exactly equal to sums of exponentials (2.35). This leads to an algorithm which is mathematically equivalent to the one proposed by Sofronov [63, 64] and Grote-Keller [28, 29, 30]:

$$\int_0^t M_\ell(c(t-\tau)/R) \begin{pmatrix} E^{(2)}_{\ell m}(R,\tau) \\ B^{(2)}_{\ell m}(R,\tau) \end{pmatrix} d\tau = \sum_{k=1}^{\ell} \mathbf{Z}_{\ell,k}(t), \tag{2.61}$$

$$\frac{d\mathbf{Z}_{\ell,k}}{dt} = \frac{z_{\ell,k}c}{R}\mathbf{Z}_{\ell,k} - \frac{z_{\ell,k}c}{R} \begin{pmatrix} E^{(2)}_{\ell m}(R,\tau) \\ B^{(2)}_{\ell m}(R,\tau) \end{pmatrix}, \quad \mathbf{Z}_{\ell,k}(0) = \mathbf{0}. \tag{2.62}$$

Now the number of auxiliary functions $\mathbf{Z}_{\ell,k}(t)$ which must be computed is proportional to λ^{-3}. Thus the cost of the local convolution algorithm is:

$$\text{Work}_{\text{conv}} \propto \lambda^{-4}T, \quad \text{Storage}_{\text{conv}} \propto \lambda^{-3}, \tag{2.63}$$

which is comparable to the work and storage required by the volume solver.

Further improvements in efficiency and generalizations to the planar and cylindrical boundaries follow from the uniform approximation of the temporal convolution kernels by a smaller number of exponentials. The analysis and practical construction of these approximations is carried out in [2, 3]. We will review their analysis briefly. However, from the user's perspective, one only needs a table of exponents and amplitudes. These can be obtained at [34].

Let $C_p(t)$ denote any of the convolution kernels derived above (see (2.15),(2.43),(2.52)) with p representing the spatial harmonic index. The approximation problem is to find $(\alpha_{j,p}, \beta_{j,p})$, $j = 1, \ldots, N_p$, such that:

$$R_p(t) = \sum_{j=1}^{N_p} \alpha_{j,p} e^{\beta_{j,p} t}, \tag{2.64}$$

satisfies for some (small) tolerance ϵ and (large) time T:

$$\|(R_p - C_p) * f\|_{L_2(0,T)} \leq \epsilon \|f\|_{L_2(0,T)}. \tag{2.65}$$

By Parseval's relation we can translate this to an equivalent statement on the rational approximation of the Laplace transform of the kernel:

$$\max_{\Re(s)=T^{-1}} |\hat{R}_p(s) - \hat{C}_p(s)| \leq \frac{\epsilon}{e}, \tag{2.66}$$

where we note that:

$$\hat{R}_p(s) = \sum_{j=1}^{N_p} \frac{\alpha_{j,p}}{s - \beta_{j,p}}. \tag{2.67}$$

The fundamental theoretical result of [2, 3] is that all the kernels admit exponential approximations with:

$$N_p \leq C \ln \frac{1}{\epsilon} \cdot \ln (pT). \tag{2.68}$$

The proof is based on representations of $\hat{C}_p$ as sums/integrals of poles over appropriate contours in the left half s-plane combined with a general approximation result for functions so represented. Using these exponential approximations the convolution algorithm now costs:

$$\text{Work}_{\text{conv}} \propto \lambda^{-3} T \ln \frac{1}{\epsilon} \cdot \ln \left(\frac{T}{\lambda} \right), \quad \text{Storage}_{\text{conv}} \propto \lambda^{-2} \ln \frac{1}{\epsilon} \cdot \ln \left(\frac{T}{\lambda} \right). \tag{2.69}$$

Now the work and storage is negligible in comparison with the requirements of the volume solver. Only the cost of the spatial transforms is formally comparable.

The practical numerical construction of the poles and amplitudes yields remarkably efficient exponential approximations. In Table 1 we list results for a tolerance of $\epsilon = 10^{-6}$. (The poles and amplitudes themselves are available at [34].) Note that we exploit the homogeneity of the plane kernel to compute k-independent poles:

$$\alpha_{j,k} = |k|^2 \alpha_j, \quad \beta_{j,k} = |k| \beta_j. \tag{2.70}$$

Also note that the zero mode for the cylinder kernel is particularly difficult to approximate, but the highers modes are essentially the same as in the spherical case.

Cylinder		Sphere		Plane
n	N_n	ℓ	N_ℓ	$\lvert k\rvert T \leq 10^4$
0	26			31
1	9			
2	6			
$3-6$	5	$0-5$	ℓ	
$7-8$	6	$6-8$	6	
$9-12$	7	$9-12$	7	
$13-19$	8	$13-19$	8	
$20-31$	9	$20-31$	9	
$32-51$	10	$32-51$	10	
$52-86$	11	$52-86$	11	
$87-147$	12	$87-147$	12	
$148-227$	13	$148-228$	13	
$228-401$	14	$229-402$	14	
$402-728$	15	$403-728$	15	
$729-1024$	16	$729-1024$	16	

TABLE 1. Poles required for exponential approximations to the nonreflecting boundary kernels with a tolerance of $\epsilon = 10^{-6}$.

2.5. **Fast time-local evaluation of the kernels II: piecewise exponential approximations.** More recently, alternative fast, low-storage algorithms for evaluating evolutional convolutions have been proposed by Schädle and coworkers [50, 49, 60]. These are based on piecewise rather than global exponential approximations to the kernel. The advantages of using piecewise rather than global approximations are that they are easier to construct and more generally applicable. The disadvantages are that the very simple convolution algorithm embodied in (2.60) must be replaced by an algorithm which is more complicated, and slightly more memory and work are required.

Concerning generality, it is shown in [60] that the only essential requirement for the applicability of the approach is that the Laplace transform of the convolution kernel, $C(t)$, be sectorial. That is, for some complex number s_0 and angle $\phi < \frac{\pi}{2}$, $\hat{C}(s)$ is analytic for $|\arg(s - s_0)| < \pi - \phi$. Moreover, for positive constants M and ν:

$$|\hat{C}(s)| \leq M|s|^{-\nu}. \tag{2.71}$$

These requirements are satisfied by the kernels $C_p(t)$ discussed above, but, of course, by many other kernels appearing in diverse applications. The exponential approximations themselves are defined on intervals of rapidly increasing length. Fixing a base, $B > 1$, and a time step Δt the kernel is approximated by a fixed number of exponentials, $P \propto \ln \frac{1}{\epsilon}$, on each subinterval:

$$C(t) \approx \sum_{j=1}^{P} \alpha_j^{(k)} e^{\beta_j^{(k)} t}, \quad t \in [B^{k-1}\Delta t, (2B^k - 1)\Delta t] \equiv I_k. \tag{2.72}$$

(Notice the overlap.) The poles and amplitudes are directly computed from $\hat{C}(s)$ by applying a P-point quadrature rule to the Laplace inversion integral along a specially chosen contour; the so-called Talbot contour [66]. For fixed B one can take $P \propto \ln \frac{1}{\epsilon}$ for an error tolerance ϵ. Thus the least squares procedure of [2, 3] is avoided, and the approximations can be computed on the fly; all the user needs to know is the singularity structure of $\hat{C}$ which determines some parameters in the contours.

The approximate convolution may be derived as follows. If the final simulation time is T it is clear that the piecewise approximations to C will eventually be needed on intervals I_k, $k = 1, \ldots, L$ where L is the smallest integer such that $(2B^L - 1)\Delta t \geq T$. Clearly $L \propto \ln(\lambda^{-1}T)$. We solve the differential equations associated with (2.72) over intervals $((\ell - 1)B^k\Delta t, \ell B^k \Delta t)$, $\ell = 1, \ldots, \ell_F$, where $(\ell_F + 1)B^k\Delta t > T$. Precisely, suppose

$$\frac{dy_{j,k,\ell}}{dt} = \beta_j^{(k)} y_{j,k,\ell} + \alpha_j^{(k)} u(t), \quad y_{j,k,\ell}\left((\ell - 1)B^k\Delta t\right) = 0, \tag{2.73}$$

and set:

$$z_{j,k,\ell,p} = y_{j,k,\ell}\left(((\ell - 1)B^k + pB^{k-1})\Delta t\right), \quad p = 1, \ldots, B. \tag{2.74}$$

Note that the work involved in computing these numbers is propoprtional to $PL\lambda^{-1}T \propto \ln \frac{1}{\epsilon} \cdot \ln(\lambda^{-1}T)\lambda^{-1}T$. Now consider the approximate evaluation of

$$\int_0^t C(t - \tau)u(\tau)d\tau. \tag{2.75}$$

Obviously the local part of the integral can be approximated using local data and so we concentrate on the integral up to $t-\Delta t$. We partition it into subintervals over which the various kernel approximations are valid. Precisely, we determine $t-\Delta t=\tau_0>\tau_1>\ldots>\tau_M=0$ such that $\tau_k=(\ell_k-1)B^k\Delta t$ for some integer ℓ_k and $(t-\tau_{k-1},t-\tau_k)\in I_k$. (The construction of the partition involves an expansion of the time step index in base B; see [49].) We then have:

$$\begin{aligned}\int_0^{t-\Delta t} C(t-\tau)u(\tau)d\tau &= \sum_{k=1}^{M}\int_{\tau_k}^{\tau_{k-1}} C(t-\tau)u(\tau)d\tau \\ &\approx \sum_{k=1}^{M}\sum_{j=1}^{P} e^{\beta_j^{(k)}(t-\tau_{k-1})}z_{j,k,\ell_k,p_k} \end{aligned} \tag{2.76}$$

where $(\ell_k-1)B+p_k=\ell_{k-1}-1$. Applying this algorithm to the nonlocal boundary conditions described above and being careful about which values $z_{j,k,\ell,p}$ can be discarded we find that the cost is:

$$\text{Work}_{\text{conv}}\propto\lambda^{-3}T\ln\frac{1}{\epsilon}\cdot\ln(\lambda^{-1}T),\quad \text{Storage}_{\text{conv}}\propto\lambda^{-2}\ln\frac{1}{\epsilon}\cdot\ln(\lambda^{-1}T), \tag{2.77}$$

which is again negligible in comparison with the volume solver.

Of course, it can be argued that these developments do not improve on the existing global approximations which have already been constructed and tabulated, and which we have seen to be quite efficient for the kernels arising in applications to Maxwell's equations. However, they can be used to evaluate exact conditions for spatial discretizations, which may prove more accurate for problems with unresolved waves of nonnegligible amplitude. This is carried out in detail in [49]. Furthermore, they may be useful for generalizations to more complex media.

3. Exact formulations on general boundaries

Despite the existence of fast, low-storage evaluation algorithms, the fact that the boundary conditions considered so far require the use of a restricted set of artificial boundaries does lead to nonnegligible costs in some cases. In particular, the need to embed a high-aspect-ratio scatterer in a spherical computational domain may drastically increase the computational requirements. Therefore one would like to construct accurate radiation conditions on more general boundaries, and we will discuss such procedures for the remainder of the article.

3.1. **Kirchhoff representations.**

Rather early on Ting and Miksis [70] proposed a scheme for implementing exact boundary conditions for the time–dependent scalar wave equation. They considered a scenario as in Figure 1, with the computational domain extended spatially and taken to lie within another artificial boundary Γ'. Provided that the initial data, $u(\cdot,0)$ and $u_t(\cdot,0)$, lies within Γ (and further that any inhomogeneities are confined both spatially and temporally to the region of Ω within Γ), then field values on Γ' have a retarded Kirchhoff representation,[9]

$$\begin{aligned}u(\mathbf{x}',t)=-\frac{1}{4\pi}\int_\Gamma\Big[&u(\mathbf{x},t-r/c)\frac{\partial}{\partial n}\left(\frac{1}{r}\right)\\ &-\frac{1}{r}\frac{\partial u}{\partial n}(\mathbf{x},t-r/c)-\frac{1}{rc}\frac{\partial r}{\partial n}\frac{\partial u}{\partial t}(\mathbf{x},t-r/c)\Big]\,dS_{\mathbf{x}},\quad \mathbf{x}'\in\Gamma'\end{aligned} \tag{3.78}$$

where $dS_{\mathbf{x}}$ is the area measure and $\mathbf{n}$ is the inward–pointing normal on Γ (that is outward–pointing with respect to the tail Ξ). Givoli and Kohen [25] numerically implemented this scheme for both the scalar wave equation in three space dimensions and for the equations of elasticity. He and Weston [42] developed a fully vector version of the scheme as applied to the Maxwell equations.

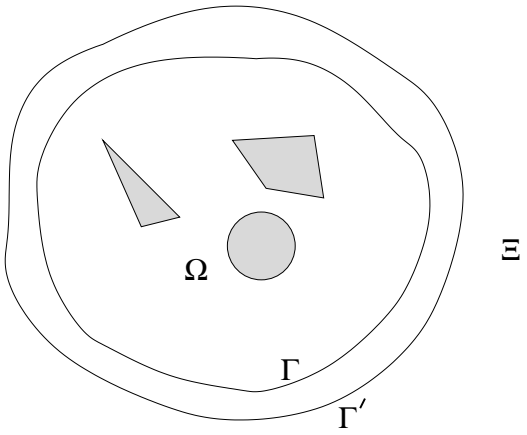

FIGURE 1. DOMAINS FOR AN EXTERIOR PROBLEM. Ξ is the tail, Ω is the computational domain, and both Γ and Γ' are artificial boundaries. The irregular objects within Ω represent scatterers.

Teng [68] demonstrated that one can do away with the need for two artificial boundaries, in effect considering the limit when Γ and Γ' are the same surface. For a generic point $\mathbf{x}' \in \Gamma$, he finds that

$$u(\mathbf{x}',t)\left(1-\frac{\Theta(\mathbf{x}')}{4\pi}\right) = -\frac{1}{4\pi}\int_\Gamma \left[u(\mathbf{x},t-r/c)\frac{\partial}{\partial n}\left(\frac{1}{r}\right)\right.$$
$$\left. -\frac{1}{r}\frac{\partial u}{\partial n}(\mathbf{x},t-r/c) - \frac{1}{rc}\frac{\partial r}{\partial n}\frac{\partial u}{\partial t}(\mathbf{x},t-r/c)\right] dS_{\mathbf{x}}, \quad \mathbf{x}' \in \Gamma, \tag{3.79}$$

where $\Theta(\mathbf{x}')$ is the exterior solid angle as measure in the tangent space at $\mathbf{x}'$. Provided that the artificial boundary is smooth at $\mathbf{x}'$, his formula reduces to

$$u(\mathbf{x}',t) = -\frac{1}{2\pi}\int_\Gamma \left[u(\mathbf{x},t-r/c)\frac{\partial}{\partial n}\left(\frac{1}{r}\right)\right.$$
$$\left. -\frac{1}{r}\frac{\partial u}{\partial n}(\mathbf{x},t-r/c) - \frac{1}{rc}\frac{\partial r}{\partial n}\frac{\partial u}{\partial t}(\mathbf{x},t-r/c)\right] dS_{\mathbf{x}}, \quad \mathbf{x}' \in \Gamma. \tag{3.80}$$

This boundary condition is clearly nonlocal in space and time; however, its history dependence is restricted in the following sense. The integral involves the retarded time $\tau = t - r/c$ which may be confined to the interval $t - r_{\max}/c \le \tau \le t$, where $r_{\max}$ is the maximum Euclidean distance between any two points on Γ.

3.2. **Origin of simple of history terms.** Teng's derivation of (3.79) relies on the theory of distributions. Although we shall not repeat his argument, let us show how such history–dependent terms arise in a restricted setting, that is the homogeneous scalar wave equation for $c = 1$ and a simple class of infinite–extent boundaries, such as an infinite plane, two semi–infinite planes which meet at an edge, or three

quarter–infinite planes which meet at a corner. We will derive a formula for $u(\mathbf{x}', T)$ at time T, with the spatial point $\mathbf{x}' = (0,0,0)$ taken as the coordinate origin and assumed common to all the planes which make up the boundary Γ. Let $B(r,t)$ represent the radius–r sphere at time t and centered at the origin. With this notation we write $B(T-t,t)$ for the intersection of time level $t < T$ and the past lightcone of the spacetime point $(0,0,0,T)$. The artificial boundary Γ divides $B(T-t,t)$ into two components, each one a *spherical polygon*, that is a spherical portion enclosed by the arcs of great circles.

For the scenario just described we will prove a lemma, and then use the lemma to produce our formula for $u(0,0,0,T)$ in the case when Γ is a single plane. Let $\mathcal{S}^*$ be the angular parameter space specifying a spherical polygon on the unit sphere, and let $B^*(r,t) \subset B(r,t)$ be the corresponding spherical polygon within the sphere $B(r,t)$. The boundary $\partial B^*(r,t)$ of $B^*(r,t)$ is a closed, continuous, and piecewise smooth curve $\gamma(r,t)$, and it may in fact be a single great circle. In any case, expressing the boundary $\gamma(r,t)$ as a union $\cup_i \gamma_i(r,t)$ of smooth curves, we use $d\sigma_i = r d\phi_i$ to represent the induced Riemannian measure (differential of arc–length) on the component $\gamma_i(r,t)$, where ϕ_i is an angular coordinate along the component. Furthermore,[1] $\partial/\partial \mathsf{x}^i$ will represent the Cartesian direction which coincides on $\gamma_i(r,t)$ with the circle's outward–pointing normal as a component of $\partial B^*(r,t)$. Along $\gamma_i(r,t)$ the vector field $\partial/\partial \mathsf{x}^i$ points perpendicularly to $\gamma_i(r,t)$ and also tangent to $B(r,t)$. Globally, $\partial/\partial \mathsf{x}^i$ is merely the normal vector field for some foliation of $\mathbb{R}^3$ into $\mathbb{R}^2$ planes. Let $\mathcal{M}$ represent the solid past null cone (or conoid) of the spacetime point $(0,0,0,T)$. For a generic time $t < T$, let $\mathcal{M}_t$ represent the closed portion of $\mathcal{M}$ lying to the future of time level t.

LEMMA: Suppose u is a classical solution to the wave equation on a neighborhood of $\mathcal{M}_t$. Then, with Φ the solid angle subtended by $B^*(r,t)$, we have[2]

$$\begin{aligned} \Phi u(0,0,0,T) = &\sum_i \int_t^T \frac{1}{T-\tau} \int_{\gamma_i(T-\tau,\tau)} \frac{\partial u}{\partial \mathsf{x}^i} d\sigma_i d\tau \\ &(T-t)\big\langle u_t \big\rangle_{B^*(T-t,t)} + \partial_T (T-t)\big\langle u \big\rangle_{B^*(T-t,t)}. \end{aligned} \tag{3.81}$$

The result can be shifted to a generic spatial point $\mathbf{x}$ by translation invariance.

To prove the lemma, we first note that the equation holds in the $t \to T^-$ limit. Indeed, in each integral over $\gamma_i(T-\tau,\tau)$ the apparently singular $(T-\tau)^{-1}$ is canceled by a $(T-\tau)$ in the $d\sigma_i$ measure. Therefore, to gather the result, we must simply establish that the right–hand side of (3.81) is constant in t. With that aim,

[1] We use the san serif x to indicate that the $\partial/\partial \mathsf{x}^i$ direction need not be one of the fixed Cartesian basis directions: $\partial/\partial x$, $\partial/\partial y$, $\partial/\partial z$.

[2] For $w = w(x,y,z,t)$ we introduce the following convention for (unnormalized) angular averages:

$$\big\langle w \big\rangle_{B^*(r,t)} = \int_{\mathcal{S}^*} w(r\sin\theta\cos\phi, r\sin\theta\sin\phi, r\cos\theta, t) dS,$$

where $B^*(r,t)$ is the radius–r spherical portion centered at the origin for which $(\theta,\phi) \in \mathcal{S}^*$. This average does *not* use the proper area measure $r^2 dS$ on $B^*(r,t)$, where $dS = \sin\theta d\theta d\phi$ is the proper area measure on the unit–sphere. By choosing not to incorporate the proper area measure in the definition of the average, we ensure that $r \to 0^+$ limits are readily taken.

we consider the following key identity:

$$(T-t)^{-1}\Delta_{S^2}u\big((T-t)\boldsymbol{\nu},t\big) = \frac{\partial}{\partial t}\left\{(T-t)u_t\big((T-t)\boldsymbol{\nu},t\big) + \frac{\partial}{\partial T}\Big[(T-t)u\big((T-t)\boldsymbol{\nu},t\big)\Big]\right\}, \tag{3.82}$$

where Δ_{S^2} is the S^2 Laplacian and $\boldsymbol{\nu} = (\sin\theta\cos\phi, \sin\theta\sin\phi, \cos\theta)$ a set of direction cosines. This identity is nothing more than the wave equation itself, here expressed in spherical polar coordinates. Indeed, note that the left–hand side of (3.82) is symbolically

$$\left(\frac{\partial}{\partial t} - \frac{\partial}{\partial R}\right) R(\mathsf{u}_t + \mathsf{u}_R + \mathsf{u}/R) = R(\mathsf{u}_{tt} - \mathsf{u}_{RR} - 2\mathsf{u}_R/R). \tag{3.83}$$

Since the angular parameter space $\mathcal{S}^*$ does not depend on time, we may integrate (3.82), thereby obtaining

$$(T-t)^{-1}\int_{\mathcal{S}^*}\Delta_{S^2}u\big((T-t)\boldsymbol{\nu},t\big)dS = \frac{\partial}{\partial t}\int_{\mathcal{S}^*}\left\{(T-t)u_t\big((T-t)\boldsymbol{\nu},t\big) + \frac{\partial}{\partial T}\Big[(T-t)u\big((T-t)\boldsymbol{\nu},t\big)\Big]\right\}dS, \tag{3.84}$$

or in our more compact notation,

$$(T-t)^{-1}\big\langle\Delta_{S^2}u\big\rangle_{B^*(T-t,t)} = \partial_t(T-t)\big\langle u_t\big\rangle_{B^*(T-t,t)} + \partial_t\partial_T(T-t)\big\langle u\big\rangle_{B^*(T-t,t)}. \tag{3.85}$$

By Stokes' Theorem, the term on left–hand side of the equation integrates to

$$(T-t)^{-1}\big\langle\Delta_{S^2}u\big\rangle_{B^*(T-t,t)} = \sum_i \frac{1}{T-t}\int_{\gamma_i(T-t,t)}\frac{\partial u}{\partial \mathsf{x}_i}d\sigma_i, \tag{3.86}$$

that is precisely minus the time derivative of the first term on the right–hand side of (3.81). Whence the right–hand side of (3.81) is indeed constant in t. □

When $B^*(T-t,t)$ is the entire sphere $B(T-t,t)$, the lemma yields the standard *spherical means formula*

$$u(0,0,0,T) = \frac{(T-t)}{4\pi}\int_{S^2}u_t\big((T-t)\boldsymbol{\nu},t\big)dS + \frac{\partial}{\partial T}\left[\frac{(T-t)}{4\pi}\int_{S^2}u\big((T-t)\boldsymbol{\nu},t\big)dS\right]. \tag{3.87}$$

We see, in some sense, that the spherical means formula holds because the "boundary of a boundary is zero" [51]. See [67] for another derivation of (3.87). We remark that the lemma above can also be established via a generalization of Hadamard's method for deriving the spherical means formula [33, 18].

When $\gamma(T-t,t)$ is the equatorial great circle lying in the plane $z=0$, the lemma yields a *hemispherical means formula*,

$$\begin{aligned} u(0,0,0,T) = {} & -\frac{1}{2\pi}\int_t^T\int_0^{2\pi}u_z((T-\tau)\cos\phi,(T-\tau)\sin\phi,0,\tau)d\phi d\tau \\ & + \frac{(T-t)}{2\pi}\int_{\mathcal{S}^+}u_t\big((T-t)\boldsymbol{\nu},t\big)dS + \frac{\partial}{\partial T}\left[\frac{(T-t)}{2\pi}\int_{\mathcal{S}^+}u\big((T-t)\boldsymbol{\nu},t\big)dS\right], \end{aligned} \tag{3.88}$$

with $\mathcal{S}^+ = \{(\theta,\phi) : 0 \le \theta \le \pi/2, 0 \le \phi \le 2\pi\}$ representing the angular parameter space specifying the northern hemisphere. If we take $t=0$ as the initial time and

further assume that the initial data vanishes for $z > 0$ (or just on a neighborhood of $B^+(T,0)$), then the last formula becomes

$$u(0,0,0,T) = -\frac{1}{2\pi}\int_0^T \int_0^{2\pi} u_z((T-\tau)\cos\phi, (T-\tau)\sin\phi, 0, \tau) d\phi d\tau. \tag{3.89}$$

A similar formula will always follow from the lemma, provided that the initial data is appropriately chosen. Since the z–derivative u_z of the solution also obeys the wave equation, the last equation holds with u replaced by u_z (again subject to our assumption about initial data). Under the integral sign, one can then exploit the wave equation in cylindrical coordinates to derive the plane boundary condition described in [35] as expressed in terms of the nonlocal operator in (2.20), although now for the plane $z = 0$ rather than $x = 0$.

3.3. **Fast evaluation of the retarded potential: the multilevel plane wave fast time domain algorithm.** The geometrical flexibility of the retarded potential formulations of exact boundary conditions is obviously attractive. In particular, unlike the formulations we have presented on symmetric boundaries, they allow one to use a computational domain of minimal size. Let us then consider the direct discretization of (3.78), as in [25], or of Teng's single-boundary reformulation (3.79) or (3.80). For each point on the boundary we must compute an integral over the boundary of data extending into the past. By our scaling assumptions this is an $O(1)$ time history independent of T. Thus the total cost of a direct algorithm is:

$$\text{Work} \propto \lambda^{-5} T, \quad \text{Storage} \propto \lambda^{-3}. \tag{3.90}$$

Thus, although the storage costs are comparable to those required by the volume solver, the work requirements are excessive. These follow from the dense matrix multiplication inherent in the discretization of the integrals. The analogous problem arises in the solution of frequency-domain integral equations of scattering theory. For the frequency-domain problem there has been an intense interest in the invention of fast algorithms to compute these dense-matrix multiplications. Important examples include the frequency-domain fast multipole algorithm (see [17] and references therein for the mathematical description and [15] for the description of a large-scale electromagnetic scattering code which uses it) and the equivalent source method (see [12] and references therein). It is natural to attempt to apply these methods in the time domain, essentially by inverting the Fourier transform. The time-domain version of the fast-multipole method is currently the best developed algorithm of this type and so we will outline it below. Equivalent source methods are discussed in the next section.

An algorithm for evaluating the retarded potential based on fast-multipole inspired ideas is the multilevel plane-wave fast time domain algorithm (PWFTD) of Michielssen et al [23, 62]. The details of its implementation are somewhat complex, so we will content ourselves with an overview, referring the reader to the original papers for more details. The fundamental ingredient in this algorithm is the efficient evaluation of space-time localized pieces of the retarded potential integral. Consider the restriction of the retarded potential integral to a small region of space-time, $S \times (t_s, t_f)$:

$$\int_S \left[u(\mathbf{x}, t-r/c) \frac{\partial}{\partial n}\left(\frac{1}{r}\right) - \frac{1}{r}\frac{\partial u}{\partial n}(\mathbf{x}, t-r/c) - \frac{1}{rc}\frac{\partial r}{\partial n}\frac{\partial u}{\partial t}(\mathbf{x}, t-r/c) \right] dS_{\mathbf{x}}, \tag{3.91}$$

where $r = |\mathbf{x} - \mathbf{x}'|$ is the distance to the target point, $\mathbf{x}'$. Clearly, this contribution is nonzero only in the time interval (T_s, T_f) with:

$$T_s = t_s + \min_{\mathbf{x}\in S} r/c, \quad T_f = t_f + \max_{\mathbf{x}\in S} r/c. \tag{3.92}$$

This remarkable property of solutions of the wave equation and Maxwell's equations in three space dimensions is referred to as the strong Huygens' prinicple or the presence of lacunae.

The basis of the PWFTD is the representation of (3.91) using propagating plane waves.[3] The mathematical basis for the time-domain plane wave representations is found in the work of Heyman [44]. He points out the fundamental fact that propagating plane wave representations are not causal; as soon as a plane wave is "turned on" the signal is felt at points arbitrarily remote from S. Thus the true signal requires in addition evanescent modes which precisely cancel these noncausal signals. However, a remarkable result of [44] is that, for the compactly supported signals considered here, regions of space-time can be identified where only the propagating waves are needed. The PWFTD algorithm employs only propagating plane waves to evaluate (3.91) at remote locations where Heyman's analysis shows they are sufficient. The outline of the basic two-level algorithm is then as follows:

- **i:** Expand the local signal into a discrete set of plane waves with directions appropriately sampled on the unit sphere.
- **ii:** Translate the planes waves to remote locations, F.
- **iii:** Evaluate the plane waves at remote nodes within F.

This basic process is then embedded in a multilevel framework. The final result is an algorithm requiring:

$$\text{Work}_{\text{PWFTD}} \propto \lambda^{-3} T \ln \frac{1}{\epsilon} \cdot \ln \frac{1}{\lambda}, \tag{3.93}$$

which is formally negligible in comparison with the volume solver. However, it seems that the constants are larger than for the other fast methods we have discussed.

4. Methods Based on Equivalent Sources

Our final example of exact, nonlocal conditions is based on the fact that solutions to Maxwell's equations in the neighborhood of our artificial boundary can be represented as the solution of the forced Maxwell system in free space, with sources distributed in the region between any scatterers or other inhomogeneities and the artificial boundary. (For example, distributed near the inner surface Γ in Figure 1.) An algorithm then follows from:

- **i:** Finding the sources;
- **ii:** Efficiently evaluating the source solution at the boundary, making use of the strong Huygen's principle (the existence of lacunae).

We remark that the retarded potential equation, particularly in the separated boundary form used in [25, 42], can be viewed as a special case. The algorithms discussed here will exploit the possibility of more flexible representations to derive efficient algorithms.

[3] A curious fact about the algorithms mentioned here is that they employ plane wave rather than multipole solution representations to achieve efficiency, but retain the word multipole in their nomenclature for historical reasons.

The most well-developed equivalent source method to date was proposed by Ryaben'kii et al [58], and applied to Maxwell's equations by Tsynkov in [71]. We first consider their construction of the sources. Define a cutoff function, $\mu(x,t)$, which equals one near and beyond the artificial boundary and zero in the region containing inhomogeneities; μ is nonconstant only in a transition region which ultimately will contain the sources. In applications to the scalar wave equation one can simply define auxiliary fields by multiplying the physical fields by μ. For applications to Maxwell's equations this direct approach is problematic as the subsequent time-decomposed sources fail to satisfy the continuity relations. Therefore, a somewhat more involved construction is advocated in [71] which we will only outline here. It entails the construction of fields $\tilde{W}$ and $\tilde{V}$ satisfying:

$$\nabla \times \nabla \times \tilde{W} = B, \quad \nabla \times \nabla \times \tilde{V} = E, \tag{4.94}$$

for x at and beyond Γ'. Then set:

$$\tilde{B} = \nabla \times \nabla \times (\tilde{\mu}\tilde{W}), \quad \tilde{E} = \nabla \times \nabla \times (\tilde{\mu}\tilde{V}). \tag{4.95}$$

By the simple application of the product rule these fields satisfy the free space Maxwell system:

$$\frac{\partial \tilde{E}}{\partial t} - c\nabla \times \tilde{B} = -4\pi\tilde{j}, \tag{4.96}$$

$$\frac{\partial \tilde{B}}{\partial t} + c\nabla \times \tilde{E} = -4\pi\tilde{j}_m, \tag{4.97}$$

as well as

$$\nabla \cdot \tilde{E} = \nabla \cdot \tilde{B} = 0, \tag{4.98}$$

$$\nabla \cdot \tilde{j} = \nabla \cdot \tilde{j_m} = 0. \tag{4.99}$$

where the artificial currents are defined via the derivatives of μ and thus are nonzero only in the transition region. The purpose of the indirect construction of $\tilde{E}$ and $\tilde{B}$ is to guarantee (4.98)-(4.99). In [71] it is shown that $\tilde{W}$ and $\tilde{V}$ may be determined only from the knowledge of the solution on Γ', but their actual construction is only described in a special case. Thus at present the optimization of this aspect of the algorithm is an open issue, and alternative methods are being studied [72]. We emphasize that for the scalar wave equation there is no issue here as the auxiliary fields can be defined simply through multiplication by μ. Of course practical applications of the method require specific choices for the cutoff function; refer to the original papers [58, 71] for specific examples.

We now address the second problem, namely the efficient evaluation of the auxiliary fields $\tilde{E}$ and $\tilde{B}$ at the artificial boundary Γ'. Recalling that these fields coincide with E and B on Γ' they can be used to provide exact boundary data of any convenient type. Here a memory-efficient algorithm is based on the presence of lacunae. Consider a current source supported in the interval (t_s, t_f). By the volume Kirchhoff integral we have, following the same reasoning as in the preceding section, that the solution is nonzero at Γ' only in the time interval $\cup_{\mathbf{x}'}(\tau_s, \tau_f)$ given by (3.92) where $\mathbf{x}'$ varies over Γ'. The details of turning this fact into an efficient algorithm are described in [59]. A sufficiently smooth partition of unity in time is introduced

to express the sources as a sum of terms with compact time support:

$$\tilde{\tilde{j}} = \sum_k \tilde{\tilde{j}}_k, \quad \tilde{\tilde{j}}_m = \sum_k \tilde{\tilde{j}}_{k,m}, \tag{4.100}$$

with the kth term supported in $(t_{s,k}, t_{f,k})$. Define $\tilde{E}_k$, $\tilde{B}_k$ to be the solution of (4.96)-(4.97) driven by the kth source. (Note that (4.99) is preserved by the time partition.) It can be solved on the finite time interval $(\tau_{s,k}, \tau_{f,k})$, on an enlarged domain with simple boundary conditions. In [58] periodic boundary conditions are recommended. Use of these enable the use of Fourier spectral discretizations which may be quite efficient.

Clearly, the computational complexity of this algorithm, at least for the scalar wave equation where construction of $\tilde{W}$ and $\tilde{V}$ are unnecessary, will be of the same order as the interior solver, (2.54). As such it may not be as efficient as some of the more elaborate constructions discussed earlier. However, again at least when applied to the scalar wave equation, it is by far the simplest exact method to implement.

More recently, Bruno and Hoch [13] have developed an alternative equivalent source algorithm for the scalar wave equation which has the potential for greater efficiency. It is essentially a time-domain version of Bruno and coworkers fast algorithm for frequency domain scattering (e.g. [12] and references therein). Its essential feature in comparison with the method described above is the use of simple sources (monopoles and dipoles) on a sparse, regular grid. It is the sparsity of the source distribution combined with the use of FFTs which leads to the potential savings. The computation of the source strengths follows from the least squares approximation to the solution data near the boundary.

5. Local approximations

Lastly we discuss what are undobtedtly the most often used techniques; the perfectly matched layer (PML) and local radiation boundary conditions. These methods provide geometric flexibility and greater potential for generalizations to inhomogeneous or even nonlinear systems. The PML in particular is extremely simple to implement. Although these methods are not directly based on exact formulations, they are convergent, albeit often nonuniformly in time. As such they are a viable alternative to the methods we have discussed, particularly if the accuracy requirements are not too stringent and the solution time, T, is not too large.

We begin with a discussion of the details of these two approaches, as well as an interesting alternative formulation which in some sense unifies them. We will then discuss their convergence properties and compare their complexity to the algorithms implementing nonlocal formulations.

5.1. **The perfectly matched layer.**

The perfectly matched layer, introduced for Maxwell's equations by Bérenger [8], is an absorbing layer with a reflectionless interface with the computational domain. Bérenger's original formulation had the defect of being only weakly well-posed, and his construction was somewhat unintuitive. Subsequently, a clearer understanding of PML as a complex coordinate stretching emerged [16]. Mathematically, the clearest formulation of PMLs for Maxwell's equations has been given by Petropoulos [54], which we follow here. For simplicity

we display his model for a Cartesian layer in the x coordinate direction. In [54] spherical and cylindrical layers are also developed.

The layer equations are most easily discussed in the frequency domain, where we will use Laplace rather than Fourier transformations. We assume the layer is located in $x \in (0, L)$. The equations then follow from the complex coordinate stretching:

$$\tilde{x} = \int_0^x \eta \left(1 + \frac{\sigma(p)}{s+\alpha}\right) dp, \tag{5.101}$$

where s is the dual variable to time. Maxwell's equations then become:

$$s\hat{E} - c\tilde{\nabla} \times \hat{B} = 0, \tag{5.102}$$

$$s\hat{B} + c\tilde{\nabla} \times \hat{E} = 0, \tag{5.103}$$

where $\tilde{\nabla}\times$ is obtained by replacing the x derivatives in $\nabla\times$ by:

$$\frac{1}{\eta}\frac{s+\alpha}{s+\alpha+\sigma(x)}\frac{\partial}{\partial x}. \tag{5.104}$$

Time-domain realizations of these equations are obtained by viewing the transformed system as an anisotropic dielectric material. The layer equations then are:

$$\frac{\partial D}{\partial t} - c\nabla \times H = 0, \tag{5.105}$$

$$\frac{\partial B}{\partial t} + c\nabla \times E = 0, \tag{5.106}$$

with the constitutive relations:

$$\frac{\partial E_x}{\partial t} + \alpha E_x = \eta \left(\frac{\partial D_x}{\partial t} + (\alpha+\sigma) D_x\right), \tag{5.107}$$

$$\eta \left(\frac{\partial E_{\tan}}{\partial t} + (\alpha+\sigma) E_{\tan}\right) = \frac{\partial D_{\tan}}{\partial t} + \alpha D_{\tan}, \tag{5.108}$$

$$\frac{\partial H_x}{\partial t} + \alpha H_x = \eta \left(\frac{\partial B_x}{\partial t} + (\alpha+\sigma) B_x\right), \tag{5.109}$$

$$\eta \left(\frac{\partial H_{\tan}}{\partial t} + (\alpha+\sigma) H_{\tan}\right) = \frac{\partial B_{\tan}}{\partial t} + \alpha B_{\tan}. \tag{5.110}$$

Thus to implement the PML one only needs to solve an additional set of ordinary differential equations. Of course one must also choose the parameters. The stretching parameter, $\eta \geq 1$, is often omitted; that is one takes $\eta = 1$. The parameter $\alpha \geq 0$ is called the complex frequency shift. Often it is set to zero, but choosing it nonzero yields enhanced long-time stability [7]. The function $\sigma(x) \geq 0$ is the absorption parameter. The error estimates described later show that $\eta \int_0^L \sigma(p)dp$ controls the error. Typically $\sigma = \sigma_0 x^q$ is used with q chosen so that the fields have sufficient differentiability properties to allow differencing across the layer interface. However, if very high order methods are used this may be a restriction. An alternative is to develop multidomain formulations with characteristic matching across the interface. Then one can choose σ to be constant, or to vanish only to first order. See, for example, [22].

Geometric flexibility arises from the implementation of the PML in domains bounded by planar faces. Then, in addition to the single-variable layer discussed above, corner layers are required. These are derived by applying the coordinate stretching in all three variables. See the appendix of [54].

Concerning the mathematical properties of the layers, strong well-posedness and stability can be established [54, 4, 6]. We note that in [4] more general PML formulations are derived based on a different viewpoint. These generalizations are necessary for the treatment of anisotropic materials.

5.2. **Convergent local boundary condition sequences.** Finally we reconsider the oldest class of domain truncation methods, local radiation boundary condition sequences. For the scalar wave equation such sequences were formulated two decades ago by Higdon [45, 46]. They have been revitalized by a number of new developments which we will discuss below. These are:

- **i:** Development of new auxiliary variable formulations allowing straightforward implementations to arbitrary order;
- **ii:** Construction of corner compatibility conditions connecting auxiliary variables at adjacent faces enabling implementations in polygonal domains;
- **iii:** Adaptive determination of boundary condition order;
- **iv:** Proofs of spectral convergence with increasing order.

Our description below will follow [39]. We note that parallel developments for the scalar wave equation are reported in [40, 24, 37].

Consider a planar artificial boundary, $x = 0$. Our starting point is a representation of the solution as a superposition of propagating and evanescent plane waves, derived under the assumption that all inhomogeneities lie in the left half plane $x \leq -\delta$ for some $\delta > 0$.

$$\begin{aligned} u(x,y,z,t) &= \int_0^{\frac{\pi}{2}} \Phi\left(ct - x\cos\theta, y, z, \theta\right) d\theta \\ &\quad + \int_0^{\infty} e^{-\sigma x} \Upsilon(y,z,t,\sigma) d\sigma, \end{aligned} \tag{5.111}$$

where u is any Cartesian field component. Following the treatment of analogous expressions in deriving the translation formulas for the fast multipole method [26], approximate (5.111) by some quadrature rule:

$$u(x,y,z,t) \approx \sum_{j=0}^{n_p-1} w_j \Phi_j(ct - x\cos\theta_j, y, z) + \sum_{j=1}^{n_e} d_j e^{-\sigma_j x} \Upsilon_j(t,y,z). \tag{5.112}$$

Local boundary conditions with $n_p + n_e$ auxiliary functions can now be constructed which are exact on this approximate representation independent of the unknown functions Φ_j and Υ_j. Recursively define for $j = 0, \ldots, n_p - 1$, again for each Cartesian component:

$$\left(\cos\theta_j \frac{\partial}{\partial t} + c\frac{\partial}{\partial x}\right)\psi_j = \left(\cos\theta_j \frac{\partial}{\partial t} - c\frac{\partial}{\partial x}\right)\psi_{j+1} \tag{5.113}$$

with $\psi_0 = u$ and for $j = 1, \ldots, n_e$:

$$\left(\sigma_j + \frac{\partial}{\partial x}\right)\psi_{n_p+j-1} = \left(\sigma_j - \frac{\partial}{\partial x}\right)\psi_{n_p+j} \tag{5.114}$$

$$\psi_{n_p+n_e} = 0. \tag{5.115}$$

Upon proving by induction that each of these auxiliary fields satisfies Maxwell's equations, one derives evolution equations along the boundary $x = 0$. Define the normal characteristic variables:

$$R_j = E_{2,j} + B_{3,j}, \quad V_j = E_{2,j} - B_{3,j}, \tag{5.116}$$

$$S_j = E_{3,j} - B_{2,j}, \quad W_j = E_{3,j} + B_{2,j}. \tag{5.117}$$

We then have for $j = 0, \ldots, n_p - 1$:

$$\begin{aligned}(1+\cos\theta_j)\frac{\partial R_{j+1}}{\partial t} + (1-\cos\theta_j)\frac{\partial R_j}{\partial t} \quad &= \\ c\left(\frac{\partial B_{1,j}}{\partial z} + \frac{\partial B_{1,j+1}}{\partial z} + \frac{\partial E_{1,j}}{\partial y} + \frac{\partial E_{1,j+1}}{\partial y}\right), \quad &(5.118)\end{aligned}$$

$$\begin{aligned}(1+\cos\theta_j)\frac{\partial S_{j+1}}{\partial t} + (1-\cos\theta_j)\frac{\partial S_j}{\partial t} \quad &= \\ -c\left(\frac{\partial B_{1,j}}{\partial y} + \frac{\partial B_{1,j+1}}{\partial y} - \frac{\partial E_{1,j}}{\partial z} - \frac{\partial E_{1,j+1}}{\partial z}\right), \quad &(5.119)\end{aligned}$$

$$\begin{aligned}(1+\cos\theta_j)\frac{\partial V_j}{\partial t} + (1-\cos\theta_j)\frac{\partial V_{j+1}}{\partial t} \quad &= \\ c\left(\frac{\partial B_{1,j}}{\partial z} + \frac{\partial B_{1,j+1}}{\partial z} - \frac{\partial E_{1,j}}{\partial y} - \frac{\partial E_{1,j+1}}{\partial y}\right), \quad &(5.120)\end{aligned}$$

$$\begin{aligned}(1+\cos\theta_j)\frac{\partial W_j}{\partial t} + (1-\cos\theta_j)\frac{\partial W_{j+1}}{\partial t} \quad &= \\ -c\left(\frac{\partial B_{1,j}}{\partial y} + \frac{\partial B_{1,j+1}}{\partial y} + \frac{\partial E_{1,j}}{\partial z} + \frac{\partial E_{1,j+1}}{\partial z}\right), \quad &(5.121)\end{aligned}$$

and for $j = 1, \ldots, n_e$:

$$\begin{aligned}\frac{\partial R_{n_p+j}}{\partial t} + \frac{\partial R_{n_p+j-1}}{\partial t} - c\sigma_j(R_{n_p+j-1} - R_{n_p+j}) \quad &= \\ c\left(\frac{\partial B_{1,j}}{\partial z} + \frac{\partial B_{1,n_p+j}}{\partial z} + \frac{\partial E_{1,n_p+j-1}}{\partial y} + \frac{\partial E_{1,n_p+j}}{\partial y}\right), \quad &(5.122)\end{aligned}$$

$$\begin{aligned}\frac{\partial S_{n_p+j}}{\partial t} + \frac{\partial S_{n_p+j-1}}{\partial t} - c\sigma_j(S_{n_p+j-1} - S_{n_p+j}) \quad &= \\ -c\left(\frac{\partial B_{1,n_p+j-1}}{\partial y} + \frac{\partial B_{1,n_p+j}}{\partial y} - \frac{\partial E_{1,n_p+j-1}}{\partial z} - \frac{\partial E_{1,n_p+j}}{\partial z}\right), \quad &(5.123)\end{aligned}$$

$$\begin{aligned}\frac{\partial V_{n_p+j-1}}{\partial t} + \frac{\partial V_{n_p+j}}{\partial t} + c\sigma_j(V_{n_p+j-1} - V_{n_p+j}) \quad &= \\ c\left(\frac{\partial B_{1,n_p+j-1}}{\partial z} + \frac{\partial B_{1,n_p+j}}{\partial z} - \frac{\partial E_{1,n_p+j-1}}{\partial y} - \frac{\partial E_{1,n_p+j}}{\partial y}\right), \quad &(5.124)\end{aligned}$$

$$\begin{aligned}\frac{\partial W_{n_p+j-1}}{\partial t} + \frac{\partial W_{n_p+j}}{\partial t} + c\sigma_j(W_{n_p+j-1} - W_{n_p+j}) \quad &= \\ -c\left(\frac{\partial B_{1,n_p+j-1}}{\partial y} + \frac{\partial B_{1,n_p+j}}{\partial y} + \frac{\partial E_{1,n_p+j-1}}{\partial z} + \frac{\partial E_{1,n_p+j}}{\partial z}\right). \quad &(5.125)\end{aligned}$$

In addition for all j:

$$\frac{\partial B_{1,j}}{\partial t} = c\left(\frac{\partial E_{2,j}}{\partial z} - \frac{\partial E_{3,j}}{\partial y}\right), \tag{5.126}$$

$$\frac{\partial E_{1,j}}{\partial t} = c\left(\frac{\partial B_{3,j}}{\partial y} - \frac{\partial B_{2,j}}{\partial z}\right). \tag{5.127}$$

We see that the structure of the recursions corresponds to the directions of the characteristics. For the outgoing characteristics, R_j and S_j, one can solve for the time derivatives with increasing j, naturally starting with the time derivatives of R_0 and S_0 which can be computed from the interior. The normal fields satisfy equations which are uncoupled in j and which thus can be solved individually. For the incoming characteristics, V_j and W_j, on the other hand, one can solve with decreasing j. We then determine the boundary condition by setting:

$$V_{n_p+n_e} = W_{n_p+n_e} = 0. \tag{5.128}$$

The combination (5.118)-(5.128) thus provides a recipe for computing the time derivatives of the incoming characteristic variables given the time derivatives of the outgoing variables. Comparing with (2.12)-(2.13) and supposing (as we always have in our numerical experiments) that $\theta_0 = 0$ we see that the nonlocal terms, $\mathcal{R}V_0$ and $\mathcal{R}W_0$, are approximated by:

$$\mathcal{R}V_0 \approx \frac{\partial E_{1,1}}{\partial y} - \frac{\partial B_{1,1}}{\partial z}, \tag{5.129}$$

$$\mathcal{R}W_0 \approx \frac{\partial E_{1,1}}{\partial z} + \frac{\partial B_{1,1}}{\partial y}. \tag{5.130}$$

Despite the lengthy description, the implementation of these conditions is straightforward. In fact (5.118)-(5.127) is simply a hyperbolic system on the boundary which can be discretized using whatever scheme is used in the interior. In [39] arbitrary-order implementations using a high-order discontinuous Galerkin method are demonstrated.

To use these conditions on polygonal domains, corner and edge compatibility conditions must be derived to provide boundary conditions for the auxiliary hyperbolic systems. This is accomplished in [39] in two space dimensions for sequences with $n_e = 0$. The construction there is somewhat ad hoc; it depends on formally introducing doubly indexed auxiliary variables satsfying the recursions on both faces, writing down the large system of equations which govern them, and algebraically eliminating all space derivatives. Experiments show that this procedure is stable and accurate up to very high order (over 100). However, it is not yet justified mathematically, and a simpler approach would be desirable.

5.3. **Implementations via optimal grids: a link between PML and local boundary condition sequences.** Lastly we mention an interesting connection between PMLs and high-order local boundary condition sequences for the scalar wave equation developed by Asvadurov et al. [5] and used later in [32]. The essential idea is to study the effective discrete Dirichlet-to-Neumann maps produced by discretization of the layer equations. One then realizes that for a fixed finite difference or finite element discretization, one can use the complete freedom of mesh location, including the possibility of choosing a complex mesh, to control the properties of this map. If the grid is chosen to agree with the complex grid stretching

of a PML, then, of course, a discretization of that PML is produced. However, other choices are shown to correspond to approximations akin to those presented above. In [5] a particular set of θ_j's is produced corresponding to optimal rational approximations under the assumption of certain distributions of propagating waves. In [32] a simpler, nonstaggered, grid is considered.

We will show how the ideas presented in [32] apply to the recursive formulation (5.113)-(5.115). Applying a Laplace transform in time, the basic idea is the recognition that if we treat the indices in these equations as discrete x node indices then the transformed recursion equations can be rearranged so that they take the form:

$$\frac{\hat{\psi}_{j+1}-\hat{\psi}_j}{\left(\frac{2c}{s\cos\theta_j}\right)}=\frac{1}{2}\left(\frac{\partial\hat{\psi}_{j+1}}{\partial x}+\frac{\partial\hat{\psi}_j}{\partial x}\right), \tag{5.131}$$

$$\frac{\hat{\psi}_{j+1}-\hat{\psi}_j}{\left(\frac{2}{\sigma_j}\right)}=\frac{1}{2}\left(\frac{\partial\hat{\psi}_{j+1}}{\partial x}+\frac{\partial\hat{\psi}_j}{\partial x}\right). \tag{5.132}$$

Thus they are formally equivalent to a discretization (via the box scheme) of the identity $\frac{\partial\hat{\psi}_j}{\partial x}=\frac{\partial\hat{\psi}_j}{\partial x}$ with grid spacings $\left(\frac{2c}{s\cos\theta_j}\right)$ and $\left(\frac{2}{\sigma_j}\right)$. This establishes a connection with PML under this particular discretization as one would simply use different, s-dependent grid spacings.

Guddati and Lim [32] go on to use this formal relationship to very simply derive corner compatibility conditions; one simply proceeds as with PML and solves using the tensor-product mapped grid. Clearly, much needs to be done to establish the mathematical validity of this rather formalistic construction. It does, nonetheless, raise interesting issues concerning the relationship of these two local approaches after discretization.

5.4. **Accuracy of the local approximations.** A direct approach to assessing the accuracy of the local approximations is to return to the Laplace domain and compute the reflection coefficient. We assume, as in the derivation of (5.111), that all inhomogeneities are located to the left of $x=-\delta$ and that the artificial boundary is the plane $x=0$. Estimating the error in terms of the reflection coefficient is a straightforward application of Parseval's relation; see [35, 36, 39] for details. Precisely, for fixed tangential wave numbers k they are given in terms of:

$$\max_{\Re s=T^{-1}}|R(s,k)|. \tag{5.133}$$

For the PML reflection coefficients are computed in many places, though often only displayed in the propagating mode regime. Here we take $\eta=1$, suppose a layer of width L terminated by normal characteristic boundary conditions, and define:

$$\bar{\sigma}=L^{-1}\int_0^L\sigma(\tau)d\tau. \tag{5.134}$$

After some straightforward algebra we find:

$$R_{\mathrm{PML}}=\left(\frac{(\tilde{s}^2+|k|^2)^{1/2}-\tilde{s}}{(\tilde{s}^2+|k|^2)^{1/2}+\tilde{s}}\right)e^{-2L(\tilde{s}^2+|k|^2)^{1/2}\left(1+\frac{\bar{\sigma}}{\tilde{s}+\alpha}\right)}. \tag{5.135}$$

Similarly, one can compute the reflection coefficient for the local boundary condition sequences [39]:

$$R_{\mathrm{BC}} = \kappa_P^2 \cdot \kappa_E^2 \cdot \left(\frac{(\tilde{s}^2 + |k|^2)^{1/2} - \tilde{s}}{(\tilde{s}^2 + |k|^2)^{1/2} + \tilde{s}} \right), \tag{5.136}$$

where

$$\kappa_P = \left(\prod_{j=0}^{n_p - 1} \frac{\cos\theta_j \tilde{s} - (\tilde{s}^2 + |k|^2)^{1/2}}{\cos\theta_j \tilde{s} + (\tilde{s}^2 + |k|^2)^{1/2}} \right), \tag{5.137}$$

$$\kappa_E = \left(\prod_{j=1}^{n_e} \frac{\frac{\sigma_j}{c} - (\tilde{s}^2 + |k|^2)^{1/2}}{\frac{\sigma_j}{c} + (\tilde{s}^2 + |k|^2)^{1/2}} \right). \tag{5.138}$$

We first note that the restriction to finite times is necessary; if we take $\tilde{s}$ imaginary the maximum reflection coefficients are one. This difficulty exists even for the nonlocal conditions on planar and cylindrical boundaries and is responsible for the $\ln T$ terms in the complexity estimates. Then for fixed T and assuming a bandlimited signal, $|k| \leq \lambda^{-1}$, it is clear that both methods converge. In particular $R_{\mathrm{PML}} \to 0$ as $L\bar{\sigma} \to \infty$ since:

$$\min_{\Re s = T^{-1}} \Re \left(\frac{(\tilde{s}^2 + |k|^2)^{1/2}}{\tilde{s} + \alpha} \right) > 0. \tag{5.139}$$

Similarly, $R_{\mathrm{BC}} \to 0$ as $n_p \to \infty$ as each term in the definition of κ_P is strictly smaller than one.

Rather than attempting to build analytic error estimates out of these expressions we will simply compute parameter values needed to meet various tolerances. We consider three cases: $T = 10$, $\lambda = 10^{-1}$; $T = 20$, $\lambda = 2 \times 10^{-2}$; and $T = 100$, $\lambda = 10^{-2}$. In the case of the PML we set $\alpha = 0.1$, $\bar{\sigma} = 1$, and only vary L. In the plots we assume that the number of points in the layer is proportional to $\lambda^{-1} L$. In practice one can decrease the resolution within the layer so that we are somewhat overpredicting the number of points required, but we won't attempt to quantify this effect.

For the boundary conditions we consider two choices.
Padé Parameters:

$$\cos\theta_j = 1, \quad j = 0, \ldots, n_p - 1, \quad n_e = 0, \tag{5.140}$$

Gauss-Radau-Rokhlin-Yarvin (GRRY) Parameters:

$$\theta_j = \frac{\pi(c_j + 1)}{4}, \quad j = 0, \ldots, n_p - 1, \tag{5.141}$$

where c_j are the left endpoint Gauss-Radau nodes on $[-1, 1]$ and

$$\sigma_j = \beta\lambda d_j, \quad j = 0, \ldots, n_e, \tag{5.142}$$

where d_j are the Yarvin-Rokhlin nodes [75]. (The Yarvin-Rokhlin nodes are tabulated in the f77 subroutine wts500.f available at www.netlib.org/pdes/multipole/.) For the experiments we chose $n_p = n_e$ and $\beta = 5$.

In Figure 2 we plot the maximum of the reflection coefficient as a function of the degrees of freedom in the boundary treatment (terms in the boundary condition or

points in the layer). These can be approximately fit with the following exponential convergence models:

$$
\begin{aligned}
\mathrm{err}_{\mathrm{PML}} &\propto \exp\left(-1.3\sqrt{\frac{\lambda}{cT}}n_l\right), \\
\mathrm{err}_{\mathrm{Pade}} &\propto \exp\left(-2.0\left(\frac{\lambda}{cT}\right)n_p\right), \\
\mathrm{err}_{\mathrm{GRRY}} &\propto \exp\left(-0.29\frac{(n_p+n_e)}{\ln\left(\frac{cT}{\lambda}\right)}\right).
\end{aligned}
\tag{5.143}
$$

Comparitive numerical experiments are presented in [39]. There we see that the actual errors are typically an order of magnitude or two smaller than predicted by the maximum reflection coefficient. We also show that the PML results can be improved on by coarsening the the layer resolution. Nonetheless, the results do follow the trends predicted by this analysis; the long-time error is worse for the traditional local Padé boundary conditions, using the PML results in significant improvements, and use of the GRRY parameters leads to significant improvements still.

Accepting the estimates in (5.143) we can finally estimate the complexity of the local boundary treatments:

$$
\begin{aligned}
&\mathrm{Work}_{\mathrm{PML}} \propto \lambda^{-\frac{7}{2}}T^{\frac{3}{2}}\ln\frac{1}{\epsilon}, && \mathrm{Storage}_{\mathrm{PML}} \propto \lambda^{-\frac{5}{2}}T^{\frac{1}{2}}\ln\tfrac{1}{\epsilon} \\
&\mathrm{Work}_{\mathrm{Pade}} \propto \lambda^{-4}T^{2}\ln\frac{1}{\epsilon}, && \mathrm{Storage}_{\mathrm{Pade}} \propto \lambda^{-3}T\ln\tfrac{1}{\epsilon} \\
&\mathrm{Work}_{\mathrm{GRRY}} \propto \lambda^{-3}T\ln\frac{1}{\epsilon}\cdot\ln(\lambda^{-1}T), && \mathrm{Storage}_{\mathrm{GRRY}} \propto \lambda^{-2}\ln\tfrac{1}{\epsilon}\cdot\ln(\lambda^{-1}T).
\end{aligned}
\tag{5.144}
$$

We see that the PML approach is acceptable except for T very large. The use of traditional local boundary conditions is only acceptable for $T = O(1)$. The new local boundary conditions, on the other hand, yield complexity estimates comparable to the nonlocal boundary conditions. Thus if it would be possible to extend the construction of corner compatibility conditions to this case it seems they would provide a fairly complete solution. However, at present the corner compatibility conditions have only been constructed for the case $n_e = 0$.

Lastly we note that exact reflection formulas have recently been derived by Diaz and Joly [20, 21] and de Hoop et al [19]. They study the scalar wave equation and use the Cagniard-de Hoop method. This somewhat restricts the parametrizations they can study. In particular only the cases $n_e = 0$ for boundary condition sequences and $\alpha = 0$ for PML are treated. In these cases the results are in agreement with those stated above.

Our numerical experiments for time-dependent problems in waveguides confirm the T-dependence in the complexity estimates above. However, for spherical boundaries they may be overly pessimistic. A detailed analysis for spherical PMLs in the frequency domain has been given by Bao and Wu [10] However, the frequency-dependence of their estimates precludes their direct application to time-domain problems. Recently, Chen has completed a time-domain analysis of spherical PMLs for the scalar wave equation [14], but it is unclear at present if the T-dependence in his estimates is optimal.

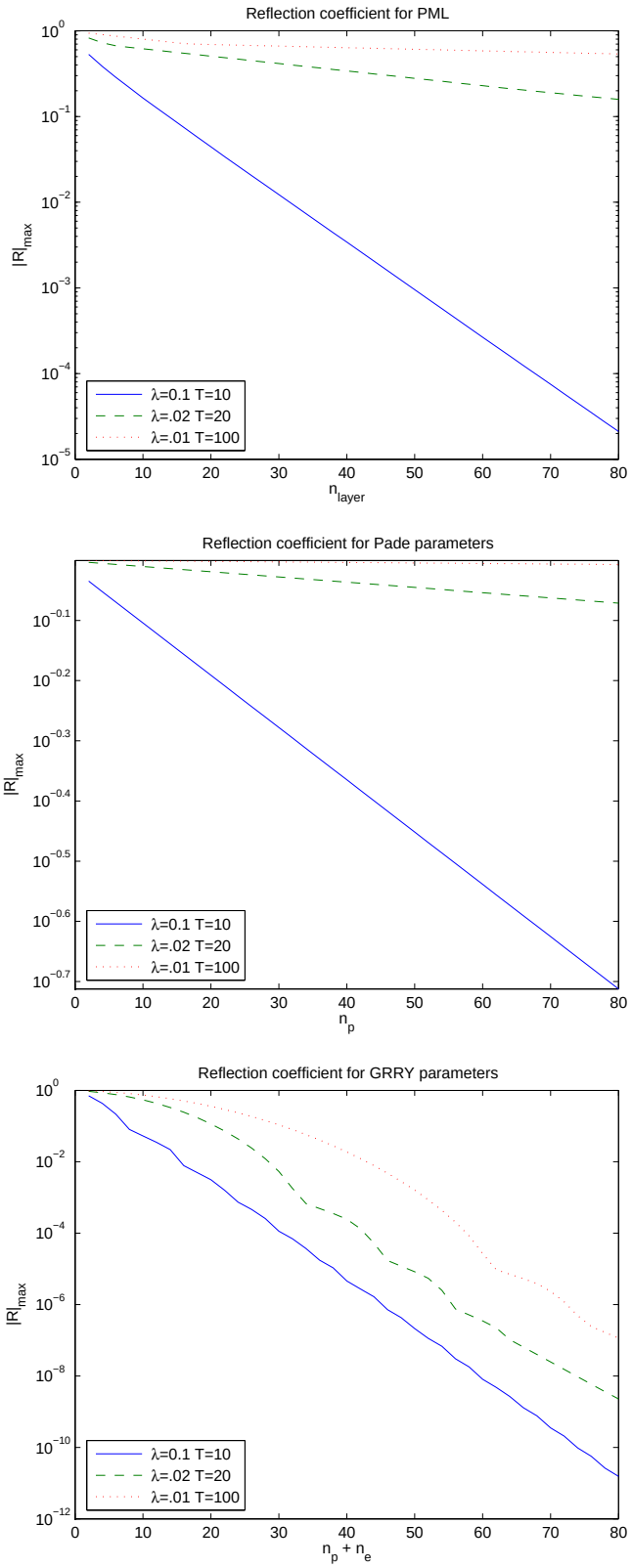

FIGURE 2. Maximum reflection coefficients for various local domain truncation techniques.

6. Epilogue: towards the ultimate solution

We have seen that there are now a number of techniques that provide completely satisfactory solutions to the time-domain radiation boundary condition problem in electromagnetics for a wide range of situations. At present, none can be called optimal for all cases considered. Although the nonlocal conditions are extremely efficient, they lack geometric flexibility. In addition, they have not been generalized to treat the important case of mutiple media extending to infinity, though it is likely that some extensions in this direction are possible. Use of the retarded potential in conjunction with the PWFTD does have favorable complexity estimates, but practical experience with the algrithm shows that there is substantial computational overhead. The perfectly matched layer does possess geometric flexibility and extensibility to more complex models. However, its accuracy can suffer in long time simulations and the issues associated with optimal numerical implementations are not easy. Local conditions based on the GRRY nodes show the most promise, but their implementation in domains with corners, which is necessary if they are to be made geometrically flexible, has yet to be demonstrated.

We finish by pointing out an interesting mathematical result due to Warchall [73]. We state it for the scalar wave equation with some simplifying assumptions; a more general version is proven in [73].

Theorem 1 (Warchall)**.** *Let $\Omega \subset \mathbb{R}^n$ be an open convex set. Let $f(x,t)$,$u_0(x)$,$v_0(x)$ be sufficiently smooth and compactly supported in $\Omega' \subset \Omega$. Finally, let u satisfy $\Box u = f$, $u(x,0) = u_0(x)$, $\frac{\partial u}{\partial t}(x,0) = v_0(x)$. Suppose $\bar{x} \in \partial\Omega$ and Δt is such that $c\Delta t < \operatorname{dist}(\bar{x}, \Omega')$. Then if $u(x,t)$ and $\frac{\partial u}{\partial t}(x,t)$ vanish for all $x \in \Omega$ satisfying $|x - \bar{x}| \leq c\Delta t$, we may conclude that $u(\bar{x}, t + \Delta t) = 0$.*

The direct interpretation of Warchall's Theorem is as follows. If we choose a convex artificial boundary such that the support of the data are located some small distance away and a time step so that the a priori domain of dependence of boundary points over a time step doesn't intersect with the support of the data, then any two solutions produced by (possibly different) data with the same support which agree on the restriction of the domain of dependence to the computational domain will have the same updated values on the boundary.

We would like to translate this local uniqueness result to a formula showing how to use the data inside Ω to update the solution. If a stable, local, exact update formula could be found, it would clearly represent the ultimate solution to the radiation boundary condition problem.

References

1. M. Abramowitz and I. Stegun, *Handbook of mathematical functions*, Dover, New York, 1972.
2. B. Alpert, L. Greengard, and T. Hagstrom, *Rapid evaluation of nonreflecting boundary kernels for time-domain wave propagation*, SIAM J. Numer. Anal. **37** (2000), 1138–1164.
3. ———, *Nonreflecting boundary conditions for the time-dependent wave equation*, J. Comput. Phys. **180** (2002), 270–296.
4. D. Appelö, T. Hagstrom, and G. Kreiss, *Perfectly matched layers for hyperbolic systems: General formulation, well-posedness and stability*, SIAM J. Appl. Math. **67** (2006), 1–23.
5. S. Asvadurov, V. Druskin, M. Guddati, and L. Knizherman, *On optimal finite difference approximation of PML*, SIAM J. Numer. Anal. **41** (2003), 287–305.
6. E. Bécache and P. Joly, *On the analysis of Bérenger's perfectly matched layers for Maxwell's equations*, Math. Model. and Numer. Anal. **36** (2002), 87–119.

7. E. Bécache, P. Petropoulos, and S. Gedney, *On the long-time behavior of unsplit Perfectly Matched Layers*, IEEE Trans. Antennas Propagat. **52** (2004), 1135–1342.
8. J.-P. Bérenger, *A perfectly matched layer for the absorption of electromagnetic waves*, J. Comput. Phys. **114** (1994), 185–200.
9. B. Baker and E. Copson, *The Mathematical Theory of Huygen's Principle*, 2 ed., Oxford University Press, Oxford, 1953.
10. G. Bao and H. Wu, *Convergence analysis of the perfectly matched layer problems for time-harmonic maxwell's equations*, SIAM. J. Numer. Anal. **43** (2005), 2121–2143.
11. J. Blatt and V. Weisskopf, *Theoretical Nuclear Physics*, John Wiley & Sons, New York, 1952.
12. O. Bruno, *Fast, high-order, high-frequency integral methods for computational acoustics and electromagnetics*, Topics in Computational Wave Propagation (M. Ainsworth, P. Davies, D. Duncan, P. Martin, and B. Rynne, eds.), Springer-Verlag, 2003, pp. 43–82.
13. O. Bruno and D. Hoch, *Exact nonreflecting boundary conditions based on equivalent sources for time dependent scattering problems*, In preparation, 2006.
14. Z. Chen, *Stability and convergence of the time-domain perfectly matched layer methods for acoustic scattering problems*, In preparation, 2007.
15. W. Chew and S. Lee, *Fast Illinois solver code (FISC)*, IEEE Ant. and Prop. Magazine **40** (1998), 19–23.
16. W. Chew and W. Weedon, *A 3-D perfectly matched medium from modified Maxwell's equations with stretched coordinates*, Microwave Optical Technol. Lett. **7** (1994), 599–604.
17. R. Coifman, V. Rokhlin, and S. Wandzura, *The fast multipole method for the wave equation: a pedestrian description*, IEEE Ant. and Prop. Magazine **35** (1993), 7–12.
18. R. Courant and D. Hilbert, *Methoden der mathematischen Physik II*, Springer-Verlag, Berlin, 1937.
19. A. de Hoop, P. van den Berg, and R. Remis, *Absorbing boundary conditions and perfectly matched layers - an analytic time-domain performance analysis*, IEEE Trans. on Magnetics **38** (2002), 657–660.
20. J. Diaz and P. Joly, *An analysis of higher-order boundary conditions for the wave equation*, SIAM J. Appl. Math. **65** (2005), 1547–1575.
21. ———, *A time-domain analysis of PML models in acoustics*, Computer Meth. Appl. Mech. Engrg. **195** (2006), 3820–3853.
22. T. Driscoll and B. Fornberg, *Block pseudospectral methods for Maxwell's equations: II. Two-dimensional, discontinuous coefficient case*, SIAM J. Sci. Comput. **21** (1999), 1146–1167.
23. A. Ergin, B. Shanker, and E. Michielssen, *Fast evaluation of three-dimensional transient wave fields using diagonal translation operators*, J. Comput. Phys. **146** (1998), 157–180.
24. D. Givoli, T. Hagstrom, and I. Patlashenko, *Finite element formulation with high order absorbing boundary conditions for time-dependent waves*, Comput. Meth. Appl. Mech. **195** (2006), 3666–3690.
25. D. Givoli and D. Kohen, *Non-reflecting boundary conditions based on Kirchhoff-type formulae*, J. Comput. Phys. **117** (1995), 102–113.
26. L. Greengard, J. Huang, V. Rokhlin, and S. Wandzura, *Accelerating fast multipole methods for low frequency scattering*, IEEE Comput. Sci. Engng. **5** (1998), 32–38.
27. M. Grote, *Local nonreflecting boundary conditions for Maxwell's equations*, Comp. Meth. Appl. Mech. Engng. **195** (2006), 3691–3708.
28. M. Grote and J. Keller, *Exact nonreflecting boundary conditions for the time dependent wave equation*, SIAM J. Appl. Math. **55** (1995), 280–297.
29. ———, *Nonreflecting boundary conditions for time dependent scattering*, J. Comput. Phys. **127** (1996), 52–81.
30. ———, *Nonreflecting boundary conditions for Maxwell's equations*, J. Comput. Phys. **139** (1998), 327–342.
31. M. Grote and C. Kirsch, *Nonreflecting boundary condition for time dependent multiple scattering*, J. Comput. Phys. (2006), To appear.
32. M. Guddati and K.-W. Lim, *Continued fraction absorbing boundary conditions for convex polygonal domains*, Int. J. Num. Meth. Engng. **66** (2006), 949–977.
33. J. Hadamard, *Lecture on Cauchy's Problem in Linear Partial Differential Equations*, Dover, New York, 1952.
34. T. Hagstrom, *Coefficients for compressions of nonreflecting boundary kernels for the wave euation and Maxwell's equations*, http://www.math.unm.edu/~hagstrom/nrbc/.

35. ———, *Radiation boundary conditions for the numerical simulation of waves*, Acta Numerica **8** (1999), 47–106.
36. ———, *New results on absorbing layers and radiation boundary conditions*, Topics in Computational Wave Propagation (M. Ainsworth, P. Davies, D. Duncan, P. Martin, and B. Rynne, eds.), Springer-Verlag, 2003, pp. 1–42.
37. T. Hagstrom, D. Givoli, M. de Castro, and D. Tzemach, *Local high-order ABCs for time-dependent waves in guides*, J. Comput. Acoust. (2006), To appear.
38. T. Hagstrom and S.I. Hariharan, *A formulation of asymptotic and exact boundary conditions using local operators*, Appl. Numer. Math. **27** (1998), 403–416.
39. T. Hagstrom, D. Justo, M. deCastro, and T. Warburton, *Experiments with arbitrary order local radiation boundary conditions for Maxwell's equations on polygonal domains*, In preparation, 2006.
40. T. Hagstrom and T. Warburton, *High-order local radiation boundary conditions: Corner compatibility conditions and extensions to first order systems*, Wave Motion **39** (2004), 327–338.
41. E. Hairer, C. Lubich, and M. Schlichte, *Fast numerical solution of nonlinear Volterra convolutional equations*, SIAM J. Sci. Stat. Comput. **6** (1985), 532–541.
42. S. He and V. Weston, *Wave-splitting and absorbing boundary conditions for Maxwell's equations on a curved surface*, Math. and Comput. in Simulation **50** (1999), 435–455.
43. D. Healy, D. Rockmore, P. Kostelec, and S. Moore, *FFTs for the 2-sphere - Improvements and variations*, J. Fourier Anal. Applic. **9** (2003), 341–385.
44. E. Heyman, *Time-dependent plane-wave spectrum representations for radiation from volume source distributions*, J. Math. Phys. **37** (1996), 658–681.
45. R. Higdon, *Absorbing boundary conditions for difference approximations to the multidimensional wave equation*, Math. Comp. **47** (1986), 437–459.
46. ———, *Numerical absorbing boundary conditions for the wave equation*, Math. Comp. **49** (1987), 65–90.
47. E. Hill, *The theory of vector spherical harmonics*, Am. J. Phys. **22** (1954), 211–214.
48. E. Hill and R. Landshoff, *The Dirac electron theory*, Rev. Mod. Phys. **10** (1938), 87–132.
49. R. Hiptmair and A. Schädle, *Non-reflecting boundary conditions for Maxwell's equations*, Computing **71** (2003), 265–292.
50. C. Lubich and A. Schädle, *Fast convolution for non-reflecting boundary conditions*, SIAM J. Sci. Comput. **24** (2002), 161–182.
51. C. Misner, K. Thorne, and J. Wheeler, *Gravitation*, Freeman, San Francisco, 1973.
52. M. Mohlenkamp, *A fast transform for spherical harmonics*, J. of Fourier Anal. and Applic. **5** (1999), 159–184.
53. R. Newton, *Scattering Theory of Waves and Particles*, McGraw-Hill, New York, 1966.
54. P. Petropoulos, *Reflectionless sponge layers as absorbing boundary conditions for the numerical solution of Maxwell's equations in rectangular, cylindrical and spherical coordinates*, SIAM J. Appl. Math. **60** (2000), 1037–1058.
55. R. Price and T. Steelhammer, *Vector spherical harmonics and their application to electromagnetism*, http://www.phys.utb.edu/~rprice.
56. T. Regge and J. Wheeler, *Stability of a Schwarzschild singularity*, Phys. Rev. **108** (1957), 1063–1069.
57. J. Ruediger, *Spectral transform shallow water model*.
58. V. Ryaben'kii, S. Tsynkov, and V. Turchaninov, *Global discrete artificial boundary conditions for time-dependent wave propagation*, J. Comput. Phys. **174** (2001), 712–758.
59. ———, *Long-time numerical computation of wave-type solutions driven by moving sources*, Appl. Numer. Math. **38** (2001), 187–222.
60. A. Schädle, M. López-Fernández, and C. Lubich, *Fast and oblivious convolution quadrature*, SIAM J. Sci. Comp. **28** (2006), 421–438.
61. M. Schwartz, *Principles of Electrodynamics*, Dover Publications, New York, 1987.
62. B. Shanker, A. Ergin, M. Lu, and E. Michielssen, *Fast analysis of transient electromagnetic scattering phenomena using the multilevel plane wave time domain algorithm*, IEEE Trans. Antennas Propagat. **51** (2003), 628–641.
63. I. Sofronov, *Conditions for complete transparency on the sphere for the three-dimensional wave equation*, Russian Acad. Sci. Dokl. Math. **46** (1993), 397–401.

64. ———, *Artificial boundary conditions of absolute transparency for two- and three-dimensional external time-dependent scattering problems*, Euro. J. Appl. Math. **9** (1998), 561–588.
65. R. Suda and M. Takami, *A fast spherical harmonic transform algorithm*, Math. Comput. **71** (2002), 703–715.
66. A. Talbot, *The accurate numerical inversion of Laplace transforms*, J. Inst. Math. Appl. **23** (1979), 97–120.
67. M. Taylor, *Partial Differential Equations: Basic Theory*, Springer-Verlag, New York, 1996.
68. Z.-H. Teng, *Exact boundary condition for time-dependent wave equation based on boundary integral*, J. Comput. Phys. **190** (2003), 398–418.
69. K. Thorne, *Multipole moments of gravitational radiation*, Rev. Mod. Phys. **52** (1980), 299–339.
70. L. Ting and M. Miksis, *Exact boundary conditions for scattering problems*, J. Acoust. Soc. Am. **80** (1986), 1825–1827.
71. S. Tsynkov, *On the application of lacunae-based methods to Maxwell's equations*, J. Comput. Phys. **199** (2004), 126–129.
72. ———, Private communication, 2006.
73. H. Warchall, *Wave propagation at computational domain boundaries*, Commun. in Part. Diff. Eq. **16** (1991), 31–41.
74. G. Watson, *A Treatise on the Theory of Bessel Functions*, 2 ed., Cambridge University Press, Cambridge, 1944.
75. N. Yarvin and V. Rokhlin, *Generalized Gaussian quadratures and singular value decompositions of integral operators*, SIAM J. Sci. Comp. **20** (1998), 699–718.

Department of Mathematics and Statistics, The University of New Mexico, Albuquerque, NM 87131

E-mail address: hagstrom@math.unm.edu

Division of Applied Mathematics, Brown University, 182 George Street, Providence, RI 02912

E-mail address: lau@dam.brown.edu